AD 744688

REPORT NO. DOT-TSC-FAA-71-25

VISIBILITY CONCEPTS AND MEASUREMENT TECHNIQUES FOR AVIATION PURPOSES

G.T. SCHAPPERT
TRANSPORTATION SYSTEMS CENTER
55 BROADWAY
CAMBRIDGE, MA. 02142

JULY 1971
FINAL REPORT

Availability is Unlimited. Document may be Released To the National Technical Information Service, Springfield, Virginia 22151, for Sale to the Public.

JUL 12 1972

NATIONAL TECHNICAL INFORMATION SERVICE

Prepared for
DEPARTMENT OF TRANSPORTATION
FEDERAL AVIATION ADMINISTRATION
WASHINGTON, D. C. 20591

Approved for public release; Distribution Unlimited

The contents of this report reflect the views of the Transportation System Center which is responsible for the facts and the accuracy of the data presented herein. The contents do not necessarily reflect the official views or policy of the Department of Transportation. This report does not constitute a standard, specification or regulation.

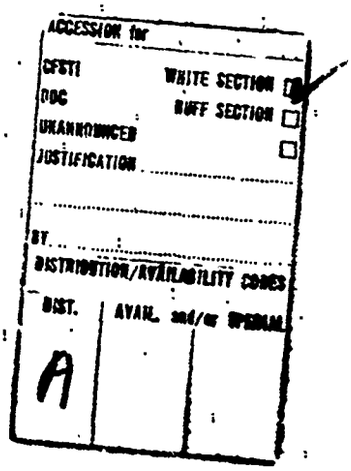

1. Report No.	2. Government Accession No.	3. Recipient's Catalog No.
DOT-TSC-FAA-71-25		

4. Title and Subtitle	5. Report Date
Visibility Concepts and Measurement Techniques for Aviation Purposes	July 1971
	6. Performing Organization Code DOT/TSC/TER
7. Author(s) G.T. Schappert	8. Performing Organization Report No.
9. Performing Organization Name and Address Optical Devices Group Transportation Systems Center 55 Broadway Cambridge, MA. 02142	10. Work Unit No. R1043 11. Contract or Grant No.
12. Sponsoring Agency Name and Address Federal Aviation Administration 800 Independence Avenue, S.W. Washington, D.C.	13. Type of Report and Period Covered Final Report 14. Sponsoring Agency Code

15. Supplementary Notes

16. Abstract This is the final report #1 of the Visibility Measuring Devices project, PPA-FA-15-Q, carried out for the Federal Aviation Administration at the Transportation Systems Center, both under the Department of Transportation.

The report reviews present techniques for measuring atmospheric transmittance and its conversion to runway visual range. The response of the pilot to visual cues used in determining the visibility is discussed as a function of his cockpit environment. The lights utilized by the FAA as targets for visibility determinations are discussed and used in the computations.

New techniques for visibility measurements and new concepts and definitions are discussed and analyzed. The emphasis is on techniques for measuring slant visual range by means of optical remote sensing devices. Various problems relating to atmospheric modeling, signal processing, and eye safety aspects are discussed.

17. Key Words	18. Distribution Statement
Visibility Runway Visual Range Atmospheric Transmission, LIDAR	Availability is Unlimited. Document may be Released To the National Technical Information Service, Springfield, Virginia 22151, for Sale to the Public.

19. Security Classif. (of this report)	20. Security Classif. (of this page)	21. No. of Pages	22. Price
UNCLASSIFIED	UNCLASSIFIED	104	

TABLE OF CONTENTS

Preceding page blank

LIST OF ILLUSTRATIONS

Preceding page blank

LIST OF ILLUSTRATIONS (Cont)

INTRODUCTION

The visibility through the atmosphere is an important consideration in the landing and take-off of aircraft. Foul weather, primarily fog and haze often cause the visibility to deteriorate so that safe landings and take-offs are not feasible. To close a major airport and divert incoming planes is a costly operation and an inconvenience to the passengers. Furthermore, under marginal visibility conditions, the airport may not be closed, but the safety of the whole operation is diminished. One way to overcome these difficulties is to employ Instrument Landing Systems (ILS) which will ultimately have the capability for fully automatic landings in zero visibility. However, such systems are not yet operational, and for the time being semi-automatic ILS landings will have to be performed. Under such conditions, the plane is brought down to 100 or 200 ft via instruments, and then under manual control to touchdown. The visibility now plays an important role both in deciding whether a landing is permitted and in preparing the pilot as to what to expect. With this in mind, it is important to have reliable and accurate visibility information for safe and economic airport operation.

The present visibility measuring system, the Runway Visual Range, or RVR system is about 20 years old. It certainly is safe and reliable within the scope for which it was intended. As its name implies, it measures the visibility along a runway. Unfortunately, this RVR is not always representative of the visibility along the glide path of an approaching aircraft, and it is this Slant Visibility which is required for successful landings. The RVR visibility is of course important once the aircraft is on the runway.

The purpose of this report is to study the feasibility of techniques which will be able to measure and monitor the slant visibility. The implementation of such techniques might lead to a system which would accurately report realistic visibility conditions on which more accurate landing decisions can be based.

In the next section of this report, we review the concepts on which the present RVR system is based. In the third section we discuss some of the possible definitions and concepts involved for Slant Visibility. In the fourth section, we discuss what we consider to be the more fruitful approaches for measuring Slant Visibility. This is followed by a conclusion. Several more detailed discussions relevant to topics in this report are relegated to the appendix.

REVIEW

Almost everyone has experienced the reduction of visibility in a dense fog, smog, or haze. This is caused by the scattering of light by the small particles which constitute the fog, smog or haze. The information signal related to "seeing" may be either the absense or presence of a light signal in a background. For an artificial light source, or an illuminated object brighter than its background, the light emitted or reflected gets scattered and less of it reaches the observer's eye. For very strong scattering (dense fog) so much of the emitted or reflected light is lost that it is no longer possible to distinguish a signal above the background and the light source or object is no longer visible. For a dark object seen against a brighter background, the light scattered into the direction of the observer may be sufficiently intense to blend in with the light background, making it impossible to distinguish the dark object, which is characterized by emitting less or no light compared to the background.

Visibility

One generally considers two different criteria in defining visibility.

1. The first criterion is the threshold of brightness contrast. An object is seen and recognized because it has a different brightness or color from its surroundings. In 1924, Koschmieder developed a theory which describes the contrast reduction due to the atmosphere. Consider an object with inherent contrast C_o with respect to the sky behind it. If such an object is viewed from a distance R, Koschmieder's theory predicts an apparent contrast C_R at the distance R

$$C_R = C_o \, e^{-\gamma R} \qquad (1)$$

where γ is the atmospheric extinction coefficient. To go from the contrast reduction to a visibility concept requires some assumption about the human visual system. Such matters will be discussed in more detail in another section and an appendix. For the present purpose all we need to know is that the limiting value of contrast e_o for the eye to be able to distinguish an object is usually taken to be $e_o = .05$. If we consider a black object against the horizon sky, the intrinsic contrast $C_o = -1$. Then, if we take the distance in Equation 1 to be so large that C_R equals the limiting contrast threshold e_o, we have the definition of the Meteorological Optical Range V

$$V = (1/\gamma) \ln 1/e_o = 2.995/\gamma \quad . \tag{2}$$

The older definitions of meteorological range uses $e_o = .02$, a value which is not in agreement with experiments.

If the "visibility" V is in miles, the extinction coefficient becomes $(\text{miles})^{-1}$. The contrast criterion for visibility is usually applicable during bright days. The value of e_o varies somewhat from observer to observer, and as we shall see later, for aviation purposes the slightly more conservative value of $e_o = .055$ is used. This results in $V = 2.900/\gamma$.

2. For some applications, the question is often at what range can one see a light source, say at night, or in a heavy fog. The limit of perception is determined by the illuminance threshold of the eye, that is, if the illuminance at the eye exceeds the threshold, the source is visible. According to Allard's law one finds

$$E_T = \frac{I}{R^2} e^{-\gamma R} \tag{3}$$

where E_T is the illuminance threshold and I the intensity of the light. Again the exponential extinction enters, together with the I/R^2 effect of a point source. The threshold illuminance E_T, a property of the eye and background lighting con-

ditions will be discussed later on. For general discussions, the visibility or meteorological range from Koschmieder's theory, Equation 2 is usually used. The definition shows the inverse relationship between the visibility V and the extinction coefficient γ, and for many purposes, this relationship is used, even though the contrast criterion may not be applicable.

The discussion so far has lumped the various physical processes which cause the extinction of light into one parameter, the extinction coefficient γ. In the visible part of the electromagnetic spectrum, scattering is usually the dominant mechanism which is responsible for the extinction coefficient, absorption may be neglected. We must now discuss the significance of this coefficient. Consider a single scattering center, for example, a gas molecule, aerosol particle or water droplet. Let us characterize the type and properties of the scatterer by a set of parameters η. These parameters can be discrete and continuous, to specify for example, a spherical water droplet of a given radius. When light of wavelength λ scatters from such a center, the process is described by a differential scattering cross-section $\frac{d\sigma}{d\Omega}(\lambda,\eta,\theta,\phi)$. This is the effective area presented by the scatterer for light which is scattered into a solid angle element $d\Omega$, centered in the direction θ, and ϕ with respect to a reference system determined by the incident light beam and the geometry of the scatterer. For complicated scatterers, there may be other angular dependences in $\frac{d\sigma}{d\Omega}$ which describe the orientation of the scatterer with respect to the incident beam parameters. Since such effects are averaged out if we consider random orientations of particles, we need not consider them at this level of the discussion. Figure 1 shows a typical geometry of a scattering act. The incident light, linearly polarized as shown is scattered into direction θ,ϕ. The polarization of the scattered light depends upon the scattering direction θ and ϕ.

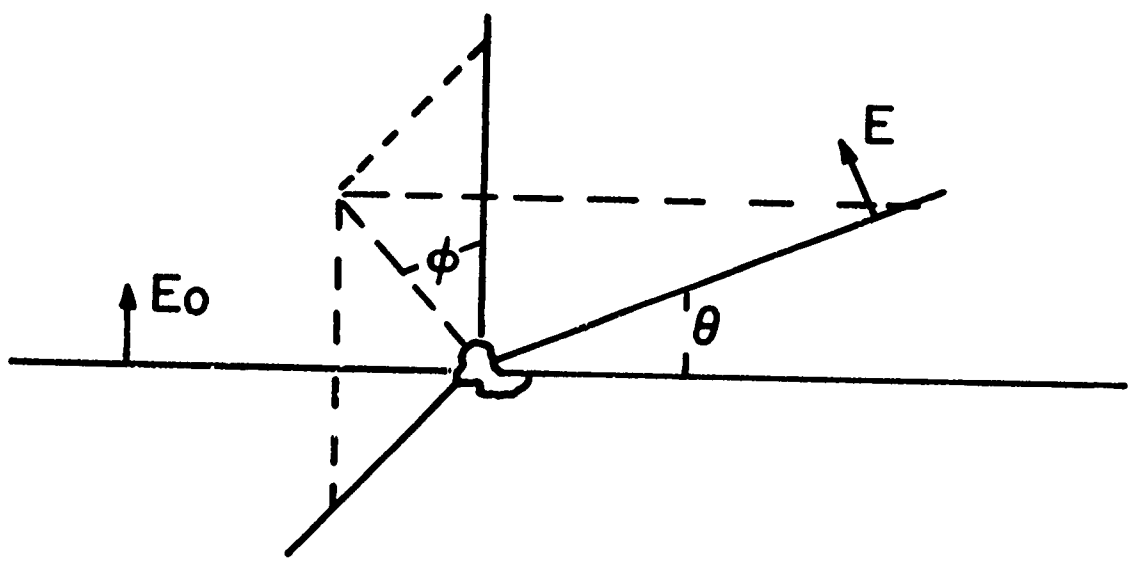

Figure 1. Geometry of Light Scattering from Single Scattering Center

The actual scattering cross-section $\sigma(\lambda,\eta)$ is the integral over all solid angles of the differential scattering cross-section. If there are $N(\eta)$ randomly distributed scatterers of type η per unit volume, they contribute $N(\eta)\sigma(\lambda,\eta)$ per unit length to the attenuation of the light beam. The total extinction $\gamma(\lambda)$ is then obtained by summing over all scatterers

$$\gamma(\lambda) = \sum_{\eta} N(\eta)\sigma(\lambda,\eta) \quad . \tag{4}$$

The above summation is in general a sum over types of scatterers, and an integral over their size distribution. In practice, it is difficult to calculate or measure the density distribution $N(\eta)$ and cross-section $\sigma(\lambda,\eta)$ separately. The total extinction $\gamma(\lambda)$ is of course easily measured. To get some feeling for the scattering mechanism and the magnitudes involved we present some qualitative arguments. In an atmosphere consisting only of atomic or molecular gases, the scattering mechanism involved is Rayleigh scattering (λ is much larger than the size of the particles.) The cross-section is easily calculated. It has the familiar λ^{-4} dependence which is partially responsible for the blueness of the sky. For a pure, dry atmosphere, one finds[1] $\gamma(.5\mu) \approx 1.7\ 10^{-5}$ (meters)$^{-1}$, which according to Equation 2 results in a visibility of about 176 Km.

At the other extreme, we might consider the extinction in a dense fog. The cross-section for scattering off a water droplet may be calculated from the Mie theory.[2] Such calculations are in general very difficult. However, if the particles are large compared to the wavelength of the light scattered, the cross-section is twice the geometric cross-sectional area. This factor of two, sometimes referred to as the "extinction paradox" is due to diffraction effects. Hence, in a fog with a mean droplet diameter of 8μ and 100 particles per cubic cm. $\gamma \approx 4\ 10^{-4}$ cm^{-1}, giving a visibility of about 100 meters. The two qualitative estimates above serve to demonstrate the orders of magnitudes involved. Clearly, the atomic or molecular con-

tributions to the extinction coefficient are negligible under ordinary circumstances.

As we have seen, all the complicated atmospheric scattering processes and particle distributions are hidden in the one parameter $\gamma(\lambda)$. For non monochromatic light, each wavelength has a different extinction coefficient, and the net extinction requires an integration over the spectral characteristic of the source. We will return to some of the details behind the extinction coefficient in a later chapter, but for the moment, we continue our review by considering the visibility as presently used and measured for aviation purposes.

Present RVR Systems

The present Runway Visual Range System was established at Newark Airport, N.J., as an ESSA - Weather Bureau program in 1956. Runway Visual Range (RVR) is defined as follows:[3,4]

> In the United States, runway visual range is an instrumentally derived value, based on standard calibrations, that represents the horizontal distance a pilot will see down the runway from the approach end; it is based on the sighting of either high intensity runway lights or on the visual contrast of other targets, whichever yields greater visual range.

This definition, as any definition of visibility, contains three essential elements:

1. The human eye which does the "seeing"
2. The target which is to be seen
3. The medium between the eye and the target.

At night, and under certain daytime conditions, the high intensity runway edge lights are the most dominant target. Under these conditions, the question is simply how far away can one of these lights be seen. From Allard's law, the illuminance E

(lumen/meter^2) from a light source of intensity I (candelas) at distance R (meters), in a medium with extinction coefficient γ (meter)$^{-1}$ is

$$E = I \frac{e^{-\gamma R}}{R^2} \tag{5}$$

If the value of E equals or exceeds the illuminance threshold E_T of the eye, the light source is visible.

To conform with the customary U.S.A. usage in the RVR system, this basic criterion for visibility is rewritten in the form

$$E_T = I \frac{(t_b)^{v/b}}{\left(v/5280\right)^2} \tag{6}$$

where v is the visual range (RVR) in ft, t_b is the atmospheric transmission over a baseline of b ft, and E_T is now in mile-candles. The relationship between the extinction coefficient γ and the transmittance t_b is simply

$$t_b = e^{-\gamma b} \tag{7}$$

where γ is in (ft)$^{-1}$ if b is in ft.

Under certain daytime conditions, the visibility of dark objects contrasted against the sky yields a greater visual range than lights. RVR is now derived from the Koschmieder theory, in which case Equation 6 is replaced by

$$e_o = (t_b)^{v/b} \tag{8}$$

where e_o is the eye's contrast threshold, all other quantities have the same meaning.

We will discuss some of the properties of the human visual system in connection with the threshold illuminance E_T and contrast threshold e_o in a later section. For the present purpose, it is sufficient to know that E_T is a function of the background brightness against which the lights are seen, and that it can vary over 6 orders of magnitude. The present RVR system singles out only two typical values:

$$\text{Day } E_T = 1000 \text{ mile-candles}$$
$$\text{Night } E_T = 2 \text{ mile-candles}$$

and takes the contrast threshold $e_o = .055$. Similarly, we will return to a discussion of the light sources and their intensity I, but for the moment it suffices to know that three intensity steps are used in the computation:

High Intensity Runway Light Settings

Step 5 I = 10,000 candelas
Step 4 I = 2,000 candelas
Step 3 I = 400 candelas

A graph of the RVR as a function of the atmospheric transmittance t_b is shown in Figure 2. The day and night curves, from Allard's Law each for three light settings, are indicated. The dotted curve, marked "contrast", is based on the Koschmieder theory. We note that for the day curves, the Koschmieder contrast curve intersects the Allard's Law curves, so that in each case the RVR value above the intersection is to be taken from the contrast curve, giving the higher value.

Another visibility definition closely related to RVR is Runway Visibility Value, RVV. This quantity is also based on Allard's and Koschmieder's Law, but the computation is based on sighting a dark object against the horizon sky during daylight, and a light of intensity 25 candelas at night.[5] The actual RVR instrumentation consists of a transmissometer to measure the

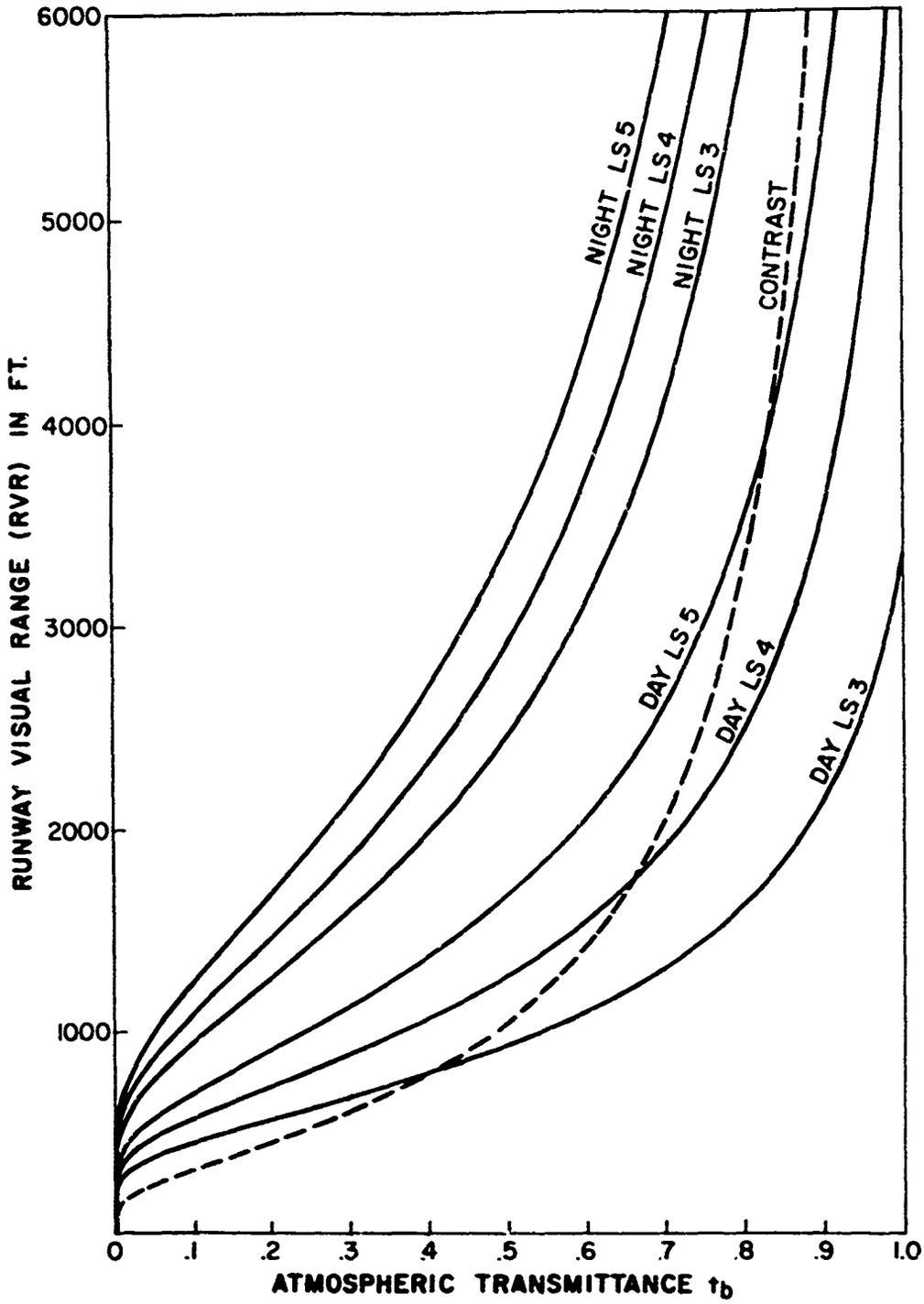

Figure 2. RVR as a Function of Atmospheric Transmittance t_b from 250 ft Baseline Transmissometer (The Solid Curves Show Allard's Law for Day and Night Illuminance Thresholds with Three Light Intensity Settings Each; the Dashed Curve Shows Koschmieder's Contrast Law)

atmospheric transmission, an indicator-recorder which indicates and records the transmittance, and a signal-data converter to compute the RVR value from the three inputs: the transmittance t_b, the light intensity setting, and the day or night E_T value. The transmissometer is a dual ended device, consisting of a light source projector which is directed to a photoelectric detector separated from the projector by a baseline of 250 or 500 ft. The light intensity is attenuated passing through the sampling path, and the light energy reaching the detector is converted into an electrical pulse train. The transmittance is then linearly related to the pulse rate, 0-4000 pulses per minute covering the transmittance from 0 - 100%. The recorder-indicator converts the pulse rate into analog voltage and values are displayed in RVV (miles and fractions to about 10 miles) and percentage transmitted. The signal data-converter, not always part of the system, computes RVR values which are displayed in hundreds feet from 0 - 6000.

The system uses a sampling period from 45 - 55 seconds, and a few seconds for computation. Hence, the RVR value is roughly a one minute average of the visibility along the baseline of the transmissometer. The present RVR system has several limitations which prevent it from giving a complete visibility picture. First, it is constrained to measure the local visibility average along its baseline. This does not give any indications of spatial inhomogeneities in the visibility, unless of course the readings from several distributed transmissometers are correlated. Second, because of the approximately one minute required for a reading, the system does not follow temporal changes in visibility shorter than one minute averages. Finally, in computing the RVR values from Allard's Law, only two threshold values for E_T as a used. Considering the 6 orders of magnitude spread of E_T as a function of the background brightness, it would seem reasonable

that the question of more steps in E_T, or possibly a continuous scale be reexamined. We will discuss this point in the next section.

Human Elements

The most difficult element to assess in the RVR system is the human visual system. Its properties enter into visibility considerations only through the two constants E_T and e_o, the illuminance threshold and brightness-contrast respectively. This appears deceptively simple. In reality, E_T and e_o depend on several factors, some of which are not readily assessed.

To begin with, E_T and e_o are related. As shown in Middleton's Vision through the Atmosphere, one can compute the point source threshold illuminance E_T from the contract threshold e. Because of this and the fact that poor visibility RVR values are more likely to be derived from Allard's Law, we will restrict ourselves to a discussion of the threshold illuminance E_T.

Appendix I is a summary of the relevant properties of the human visual system necessary for the detection of point sources from aircraft. Perhaps the most important factor is the dependence of the illuminance threshold on the background luminance. Figure 1 in Appendix I shows the variation of E_T with the background luminance B. The spread in E_T is about 6 orders of magnitude from the lowest night background to that of a bright day. In view of this, it is surprising that only a typical day value of 1000 mile candles and a night value of 2 mile candles are considered sufficient.

To assess the effect of variation in E_T on the reported RVR values, we have plotted on Figure 3 RVR as a function of log E_T for transmittance t_b from .1 to .9. The present day and night E_T values are indicated. The calculation used Allard's Law for a runway light setting LS-5 of 10,000 candelas. A 250 ft base-

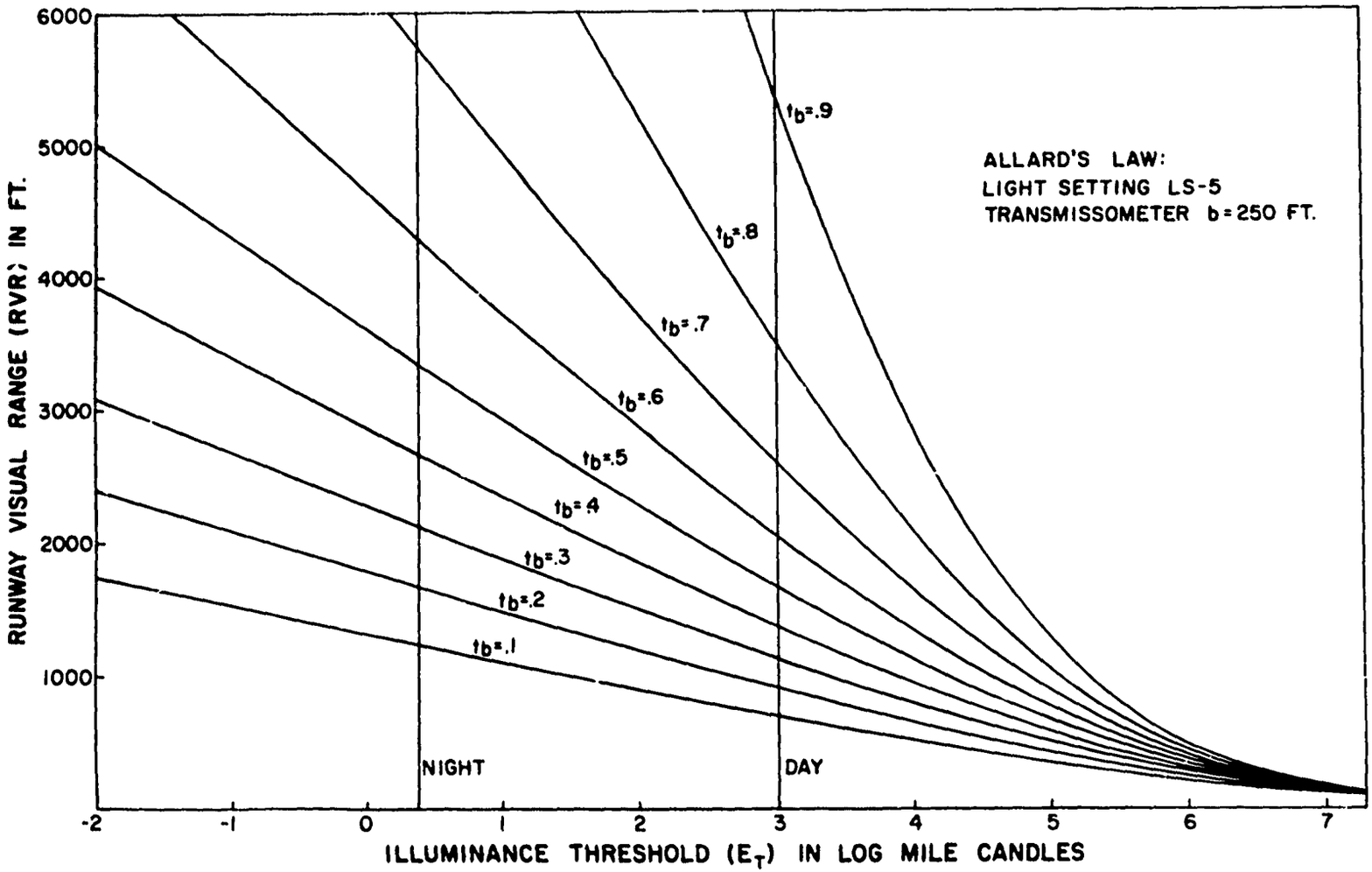

Figure 3. RVR as a Function of Log Illuminance Threshold from Allard's Law with Light Setting LS 5 for Various Atmospheric Transmittances t_b from a 250 ft Baseline Transmissometer (The Day and Night E_T Values are are Indicated by the Vertical Lines)

line is assumed for t_b. The transition from Allard's Law to Koschmieder's Law is not shown on this plot, since it itself would depend on E_T. Furthermore, since the variation of E_T is entirely due to the variation of the background luminance, the contrast threshold in Koschmieder's Law would also vary with background, although not much during daylight. The complete RVR vs background effect involves the empirical E_T and e_o vs background luminance relation. We will investigate this problem in a later report. Clearly, for t_b values below .8, LS-5, and the E_T = 1000 mile candle value (Figure 2), we are in the Allard's Law regime. Figure 3 then shows that the RVR value for t_b = .5 increases by about a factor of 2 (1675 ft to 3350 ft) between the day and night E_T value. This indicates that a greater variety, or continuous monitoring of the background luminance should be incorporated into the system. This also seems to be the position of the International Civil Aviation Organization.

Since the threshold illuminance E_T (or ϵ) is the only characterization of the human factors element which enters the visibility problem, it is important to realize that this one number must include all characteristics of the observer related to the task of detecting a light source. The classic studies on E_T vs. B by H. R. Blackwell[6] or H. A. Knoll, R. Tousey and E. O. Hulburt[7] were performed under ideal laboratory conditions. The test subjects were expected to perform one task; to detect one light source under a controlled luminance background. The resulting empirical relationship was well defined, for a given background the statistical spread in E_T was only about $\pm$ 1 dB.

For a pilot or co-pilot, during a landing, the situation is quite different. First of all, he is involved in other tasks besides concentrating on detecting a runway or approach light,

he is probably not as relaxed as a laboratory subject, and his target is a pattern of lights. To assess these strictly human factors is a difficult task. In a report An Analysis of Runway Visual Range[8], 1966, an attempt to measure E_T values under more realistic conditions was made. Observers on the back of a truck on a runway were asked to count how many runway lights they could detect. From Allard's Law, light settings and transmissometer readings, one can then calculate the E_T values. From background luminance measurements one can then compare this study to the above mentioned laboratory studies.

The runway tests resulted in E_T values with a spread of about six orders of magnitude, and surprisingly, a dependence on the runway light setting. (Figure 2, Appendix I.) If the background luminance was not preperly included in reducing the data, the six order of magnitude spread in E_T may simply reflect the dependence of E_T on the background luminance. On the other hand, if the atmospheric transmission t_b was not precisely known during the moment when the observation was made, it too could lead to a large error in E_T.

A more realistic experiment on the threshold illuminance E_T vs background luminance B was performed by the Blind Landing Experimental Unit (BLEU), a part of the Royal Aircraft Establishment. The experiment consisted of actual flights and landings in fog. The results did not agree with Blackwell's E_T vs B relationship (after adjustment for increased probability of detection). The difference is less than an order of magnitude, and may be explained by noting that a pilot's threshold is probably somewhat higher than that of a laboratory subject because he has a shorter decision time available.[9]

The effects of search time on the visibility from aircraft has recently been reported by C. A. Douglas.[10]

From Figure 3 we see that for example a half order of magnitude difference in E_T can result in a 500 ft difference in RVR for $t_b = .7$. This is out of a day value of 2700 ft or a night value of 5700 ft, and is significant if the desired reporting increment in these ranges is to be 500 ft. A distinction between the BLEU and Blackwell data in the present RVR system would be superfluous since the variable background has a much larger effect. However, in a future system, where the background is properly included, the relevance of the BLEU or Blackwell E_T vs. B relationship should be considered.

Lighting Systems

The last element of the RVR system we wish to consider is the light source which serves as the target in the visibility calculations. The only characteristic of these lights which enters the calculation in Allard's Law is their luminous intensity (candle power) in candelas. For RVR calculations the high intensity runway lights (HIRL) are used, which may be operated at ratings of 10,000, 2,000, and 400 candelas, corresponding to HIRL Steps 5, 4, and 3 respectively.

Since the candlepower is the only characteristic of these lights which enters into the RVR system, we briefly mention what factors might influence this quantity, and hence the RVR. To begin with, even new lamps have a statistical spread in their rated candlepower.

When the lamps are installed, slight missalignment can cause a less effective candlepower rating because the beam is not pointed in the right direction and one is off to the side of the beam profile. Dirt splashed on the lamps and deterioration with age are further factors which reduce the intensity.

Since the present RVR system does not monitor the HIRL lamps, the computation of RVR from Allard's Law is based on one of these standard intensities. The correct RVR value should of

course be based on the actual lamp intensity. How much of an effect a variation in the light intensity has on the RVR value is shown in Figure 4. Here we have plotted the runway visual range in ft as a function of the light intensity in candelas for typical atmospheric transmittances t_b for day (dashed lines) and night (solid lines) thresholds. The calculation is based on Allard's Law, the transmissometer base for t_b is taken as 250 ft and the standard day and night E_T threshold is used. The circled numbers indicate the intensity (candlepower) of the three standard light settings. We note in passing that since Allard's Law involves only the ratio E_T/I where E_T is the illuminance threshold and I the lamp intensity, effects due to changes or errors in E_T and I are simply related. We have treated them separately, and have plotted separate curves showing the effects on RVR because the ranges of the E_T and I variations differ by several orders of magnitude.

Two of the day curves, $t_b = .7$ and .5 end abruptly at low light intensities. This is because Allard's Law would not apply. Further, we have not plotted a $t_b = .9$ day curve, again, we would be in the Koschmieder regime.

Figure 4 demonstrates the significant fact that RVR is not a very sensitive function of the light intensity. The same conclusion can be obtained from differentiating Allard's Law, Equation (1), and expressing the derivative in the form

$$\frac{dI}{I} = \frac{dV}{V}\left(2+\frac{V}{b}\ln 1/t_b\right) \qquad (9)$$

The expression in parenthesis is always greater than 2, so that the percentage error in RVR is at most one half the percentage error in the light intensity. Assuming, that the HIRL lamps are kept clean, aligned, and not deteriorated much below about 80-90% of their rated output, they should not distort RVR values by more than a few percent.

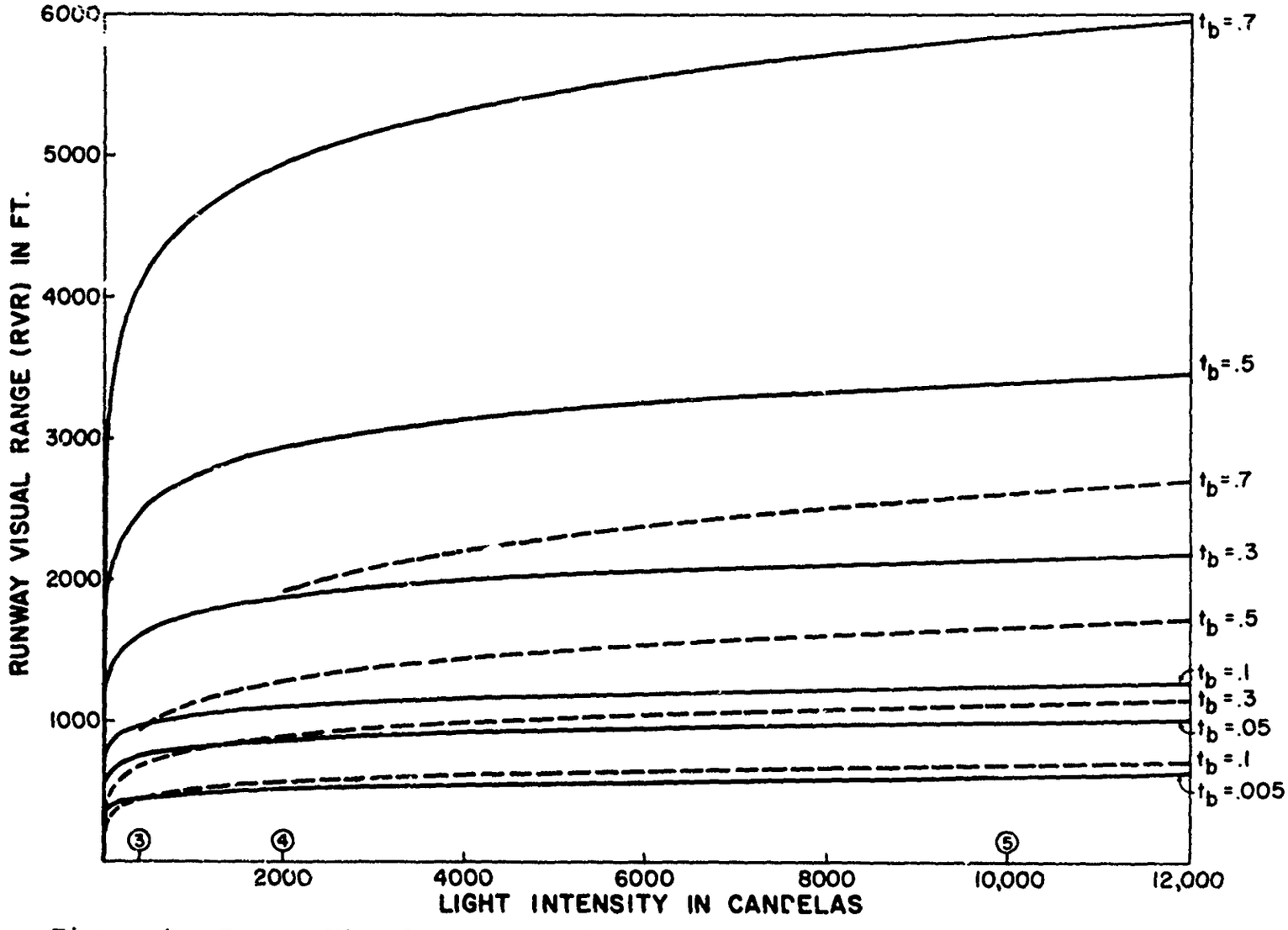

Figure 4. Runway Visual Range (RVR) in ft as a Function of Light Intensity in Candelas for Various Atmospheric Transmittances t_b Under Day (Dashed Curves) and Night (Solid Curves)(The Circled Numbers Indicate the Three Standard Light Settings.)

The differential formulation in Equation (9) is of course only valid for small $dI/_I$. If large deviations in the lamp intensity occur, the effect on the RVR values is easily read from Figure 4.

NEW CONCEPTS AND SYSTEMS

Concepts

The problem with the Runway Visual Range system described in the previous chapter is that it is applicable only to visibility along the runway. During uniform homogeneous visibility conditions, one measurement would suffice to describe the whole visibility picture. However, during inhomogeneous or rapidly varying visibility conditions, the RVR along the runway may be quite different from visibility conditions encountered by the pilot during the final approach.

Since the decision to continue a landing requires visual cues at some decision height, a measure of the visibility along the glide path of the aircraft would be advantageous. The measured visibility along a slant path would be an important input in exercising strict ground control, the so-called "tactical approach", or be useful advisory information to the pilot, the "strategic" approach.

So far, no equipment to measure the visibility along the slant path is operational. There are at least three concepts which apply to visibility along a slant path. The first definition is a natural extension of the RVR definition, that is the atmospheric path sampled is to be along the slant glide path, and the target lights are the approach lights. The calculated visibility is referred to as the slant visual range (SVR), and it is the preferred Internation Civil Aviation Organization (ICAO) definition. One difficulty with this definition is that there is no unique slant path to which it applies. The 3° glide path is not the direction in which the pilot would look for approach lights, since the glide path intersects the runway 1000 ft down from threshold. For our purposes, we interpret

SVR in the broader sense, that is, the visibility along any slant path.

To avoid this ambiguity, two other concepts relating to slant visibility have been considered by the U.S. Department of Transportation, Federal Aviation Administration.[11]

1. Visual Guidance Segment (VGS) from 100 ft.

> The length of a segment of approach lights (expressed as a distance in hundreds of feet) which a pilot will see at an altitude of 100 feet on the approach path without regard to cockpit cutoff angle.

This definition is referred to as SVR in 11. To avoid confusion with the ICAO meaning, or the broader concept of slant visual range, the more descriptive title of VGS has been recommended.

2. Approach Light Contact Height (ALCH)

> The height at which a pilot will see and should continue to see a minimum of five light bars of approach lights at 100-foot spacings, if extended to touchdown. (This assumes the approach lights are extended indefinitely at the same spacing and intensity.) A standard cockpit cutoff angle of 15 degrees shall apply.

Both of the above definitions are simply a variation of a general SVR, that is, different aspects of the geometry involved are emphasized.

To perform the calculations necessary to relate the definitions of VGS and ALCH to atmospheric visibility conditions, we need some characteristics of the approach lights which serve as the point source targets. The FAA specifications[11] define the Approach Light System (ALS) as follows:

> ALS lamps - The system is to be designed with the Q20/PAR 56 approach light system (ALS) lamps which are rated at 300 watts and have the following beam dimen-

sions. The horizontal spread angle of 30 degrees is 15 degrees from either side of the vertical plane containing the beam axis.

The vertical spread angle of 11 degrees is 5-1/2 degrees above and below the horizontal plane containing the beam axis. The average intensity within the beam region as described above for the highest three light setting steps is as follows:

Light setting 5	18,000 candelas
Light setting 4	3,600 candelas
Light setting 3	720 candelas

We can now relate VGS and ALCH definitions to the appropriate slant visibility. Figure 5 shown the geometry involved to calculate VGS. The distance SVR is the visibility along the slant path, equal to the most distant approach light visible according to Allard's Law. The closest light visible differs for the two definitions. In VGS no regard is given to cockpit cutoff angle, so the closest visible light is considered to be vertically below the plane. At 100 ft altitude on a 3° glide slope, the aircraft is just about directly above the beginning of the approach light system, which extends 1,000 ft away from the runway threshold. For ALCH, the closest light visible is where the 15° cockpit cutoff line of sight V_o intersects the light pattern as shown on Figure 5.

The distance SVR is determined from Allard's Law in the same way as for RVR. However, the lamp intensities I are different, and the atmospheric transmittance t_b is to be measured along the slant path, with b as the reference distance. Unless we have perfectly homogeneous conditions, the t_b values cannot be taken from a dual ended ground based transmissometer, but a separate device must actually sample the visibility along a slant path. How this may be accomplished will be discussed in the next sections.

From Figure 5 one easily derives the relationship

$$(SVR)^2 = (VGS)^2 + (100)^2 \qquad (10)$$

which together with Allard's Law for the visibility SVR determines VGS. The results of this calculation for the three ALS light intensities and the typical day and night illuminance threshold of 1,000 and 2 mile candles respectively are plotted on Figure 6. To compare these results with the RVR calculations, we have based the atmospheric transmittances on a 250 ft reference path.

A similar calculation yields the ALCH value. The closest visible light is determined by the 15° cockpit cutoff angle. From the geometry shown on Figure 5 we have

$$(SVR)^2 = (ALCH)^2 + (500 + ALCH \cot 15°)^2 \qquad (11)$$

which together with Allard's Law for SVR gives ALCH. The results of this calculation for the three ALS intensities and the day and night illuminance threshold are shown on Figure 7. Again, the atmospheric transmittance t_b is relative to a 250 ft reference path.

Comparing the definitions for VGS and ALCH, we note that VGS does not involve the cockpit cutoff angle, but ALCH does. This means that the VGS value is not the actual visual segment which can be seen, since it includes the segment below the cockpit cutoff. For a cutoff angle of 15°, this segment is 100/tan 15° = 373 ft. In other words, for a plane with a 15° cockpit cutoff, a VGS of 350 ft implies that no approach lights are visible. To assess the difference between a cockpit cutoff and the straight vertical downward view, we have plotted VGS for both cases for a day and night case with approach light setting 3. This is shown in Figure 8. The difference is of course always 373 ft the cockpit cutoff case giving a smaller VGS.

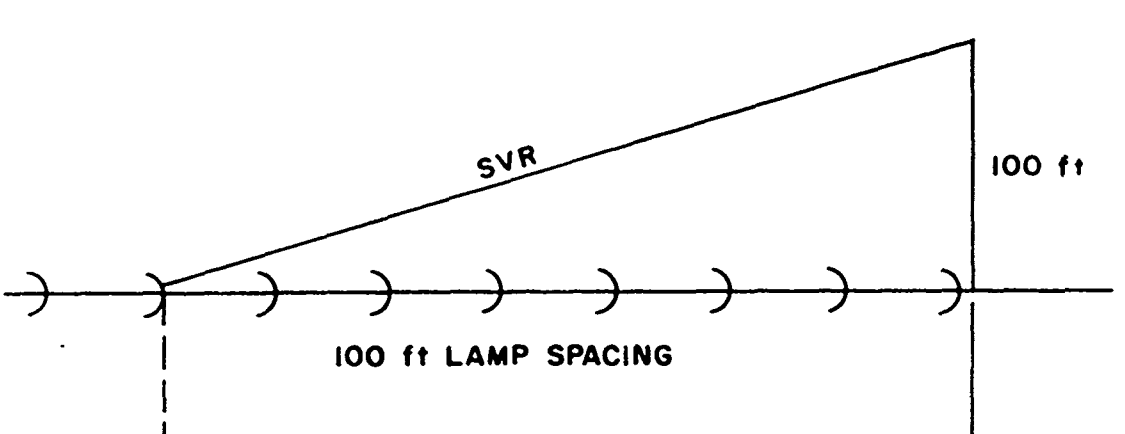

a) VGS GEOMETRY

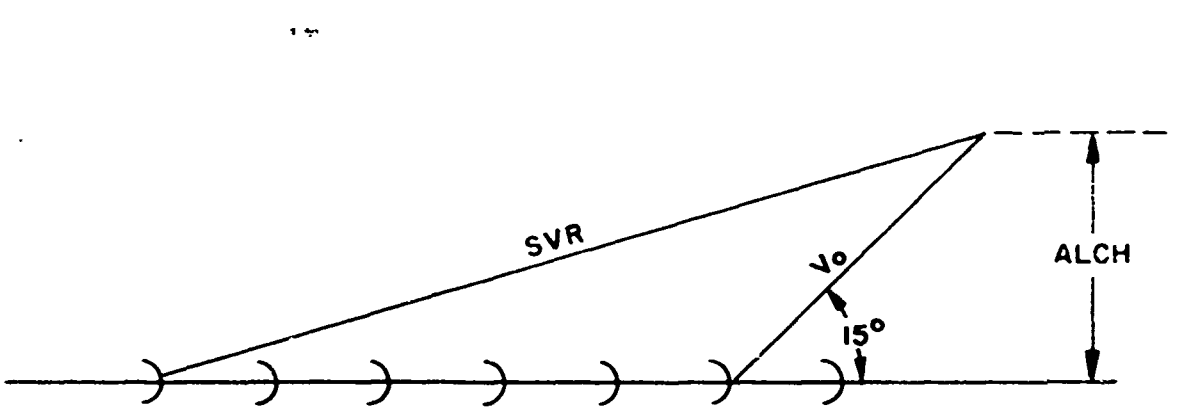

b) ALCH GEOMETRY

Figure 5. Geometry of the Visual Guidance Segment (VGS) (a) and Approach Light Contact Height (SVR) (b) Visibility Definitions. (The Distance is the Actual Alland's Law Visibility Along a Slant Path)

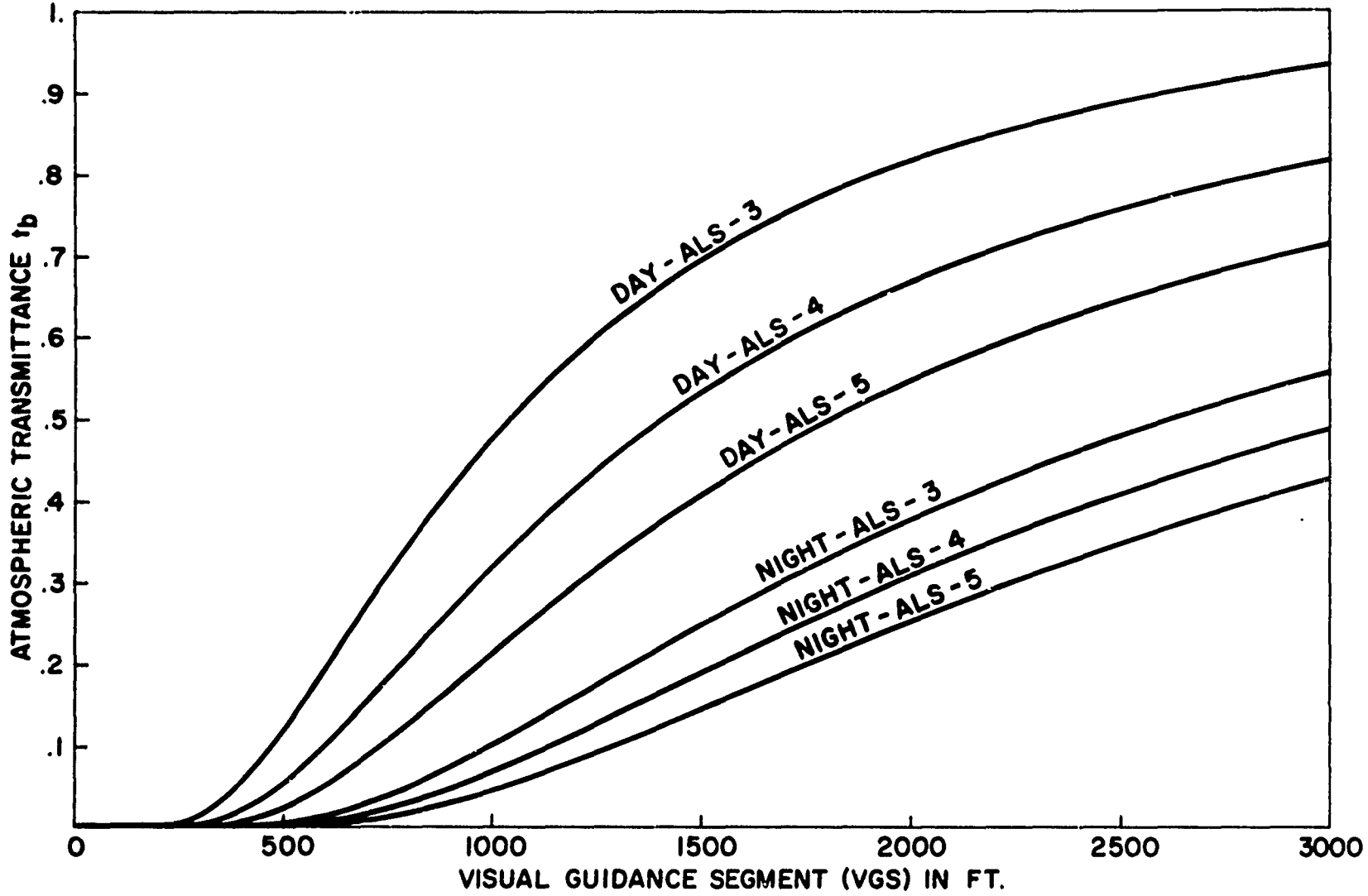

Figure 6. Visual Guidance Segment from 100 ft (VGS) vs. Atmospheric Transmittance t_b for Three Approach Light Settings and the Day and Night Illuminance Threshold

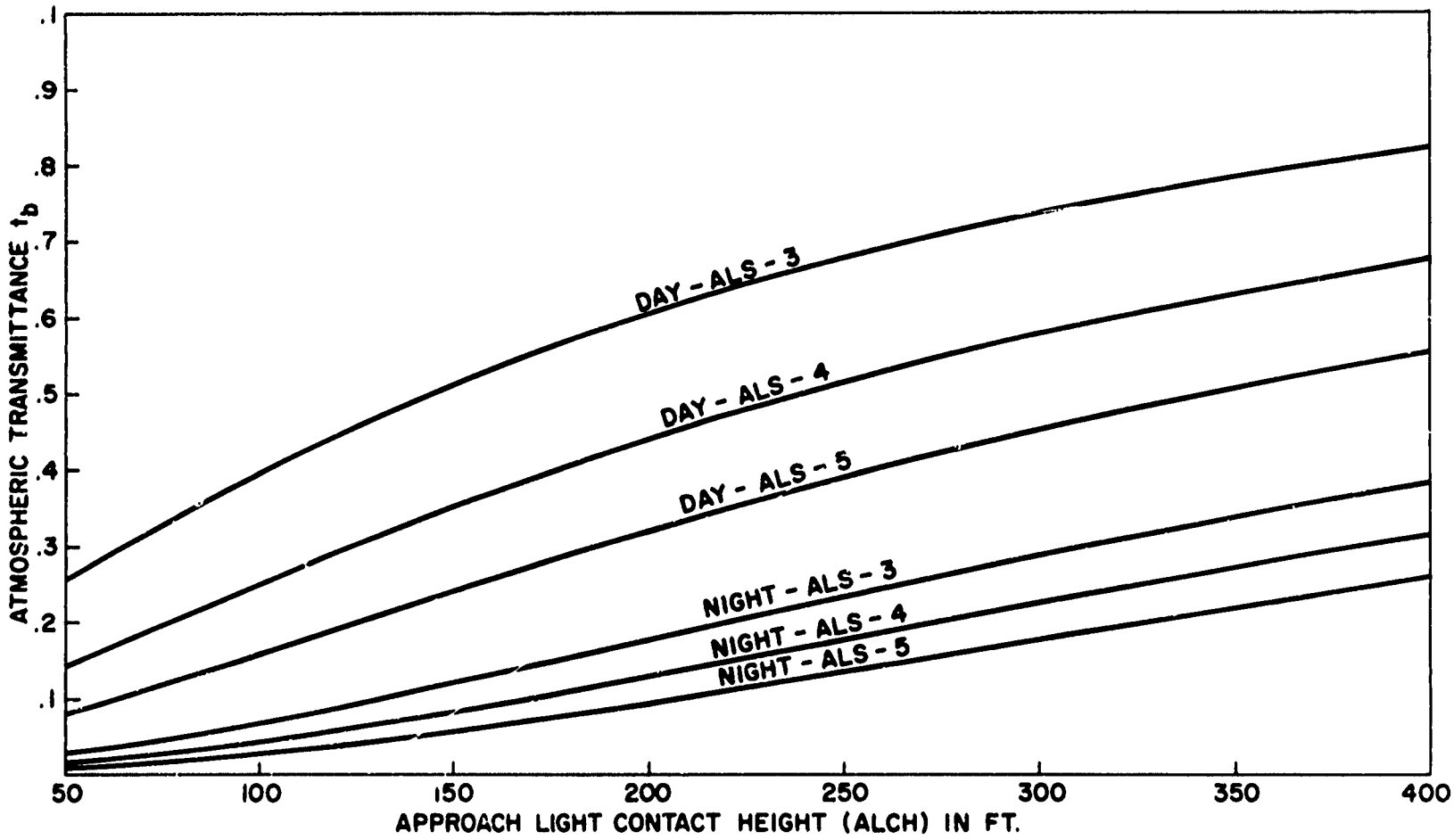

Figure 7. Approach Light Contact Height (ALCH) vs. Atmospheric Transmittance t_b for Three Approach Light Settings and the Day and Night Illuminance Threshold

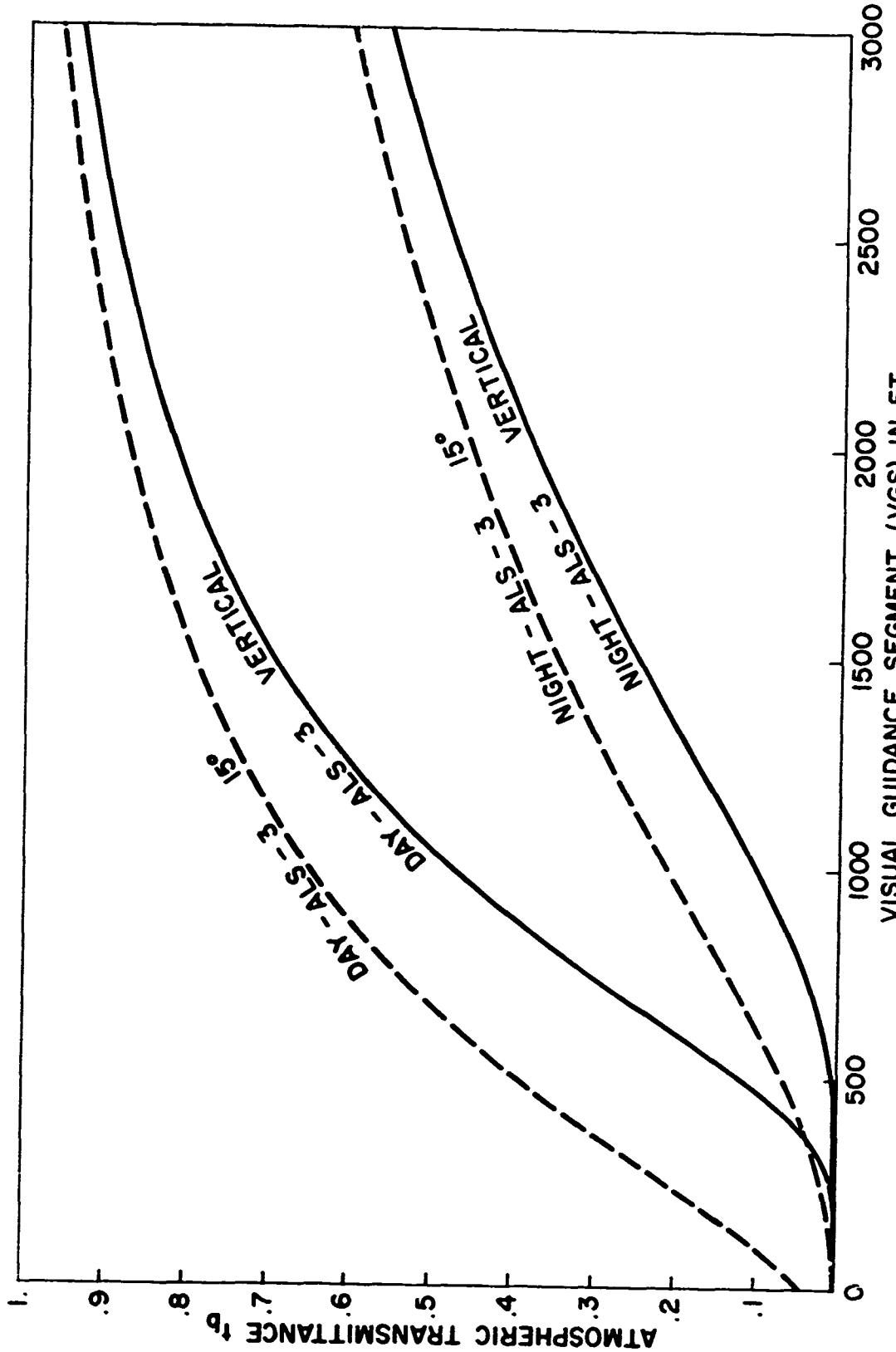

Figure 8. Effects of Cockpit Cutoff Angle on the Visual Guidance Segment (VGS). (A 15° Cockpit Cutoff Angle (Dashed Curve) is Compared with the Vertical Downward Viewing Case (Solid Curve) for the Day and Night Threshold Illuminance with Approach Light Setting 3.)

Since the cocpit cutoff angle and the angle of attack of various aircraft differ, the actual ALCH value and the actual visual guidance segment seen would always depend on the aircraft. In view of this, it might be advisable to report a VGS value (independent of cockpit cutoff) and have a correction factor for each aircraft. Such a correction is not as easily applied to the ALCH definition. Except for the cockpit cutoff effect, it is not obvious which definition is more suitable from a operational point of view. Since the actual visibility measurement SVR is the same in both cases, the difference reduces simply to the geometry.

Systems

At the present time there is no operational equipment to measure visibility along the slant path. Any detailed discussion of a system at this point would be premature. However, it is important to realize what some of the building blocks of a Slant Visual Range system are. Basically, we consider the system to consist of three essential elements:

1. Sensors, to perform the necessary measurements
2. A computer, to evaluate the measurements and calculate appropriate quantities
3. Displays which present the required information.

The most crucial component of this system is the sensor which measures the atmospheric transmittance along the glide path. Clearly, dual ended devices, like a transmissometer with several hundred feet separation are not suitable for this purpose. Locating any device at some altitude in the vicinity of the glide slope would interfere with aircraft operation. This leaves the possibility of an indirect measurement of atmospheric transmittance or a direct measurement from ground to approaching aircraft. This second technique may be envisioned in several configurations. The intensity of a light source on the aircraft

is measured on the ground, or vice versa, the intensity of an approach light is measured from the aircraft. Television, or other optical imaging devices could be employed. However, any such system can furnish visibility information only at the instant when the aircraft is in some appropriate range, which depends on the visibility. In reduced visibility conditions, it will in general be too late to make either tactical or strategic use of the information. For this reason, we will concentrate on indirect measurements of visibility. The technique in this case is based on the fact that the particles in the atmosphere reduce the visibility by scattering light out of the line of sight. The more light scattered, the pooror the visibility. By measuring this scattered light, one gets some measure of the visibility. The theory and measurement techniques of this phenomenon are the subject of the next Chapter. From a systems point of view, all one requires is a sensor to measure atmospheric transmittance.

Because of the threshold illuminance's dependence on the background luminance, it is advisable to have a sensor to measure the background. This information is then included in the visibility calculation. As we mentioned in the RVR system review, replacing the background by just the two typical day or night values is probably the largest source of error. This correction should be of top priority in any future system. The measurements from the background luminance sensor and the atmospheric transmittance sensor are then fed into a special purpose computer, the visibility (for a given definition) is calculated and transmitted to displays at locations where this information is needed. A block diagram of the basic elements is shown on Figure 9. We have included the present RVR measurements for completeness.

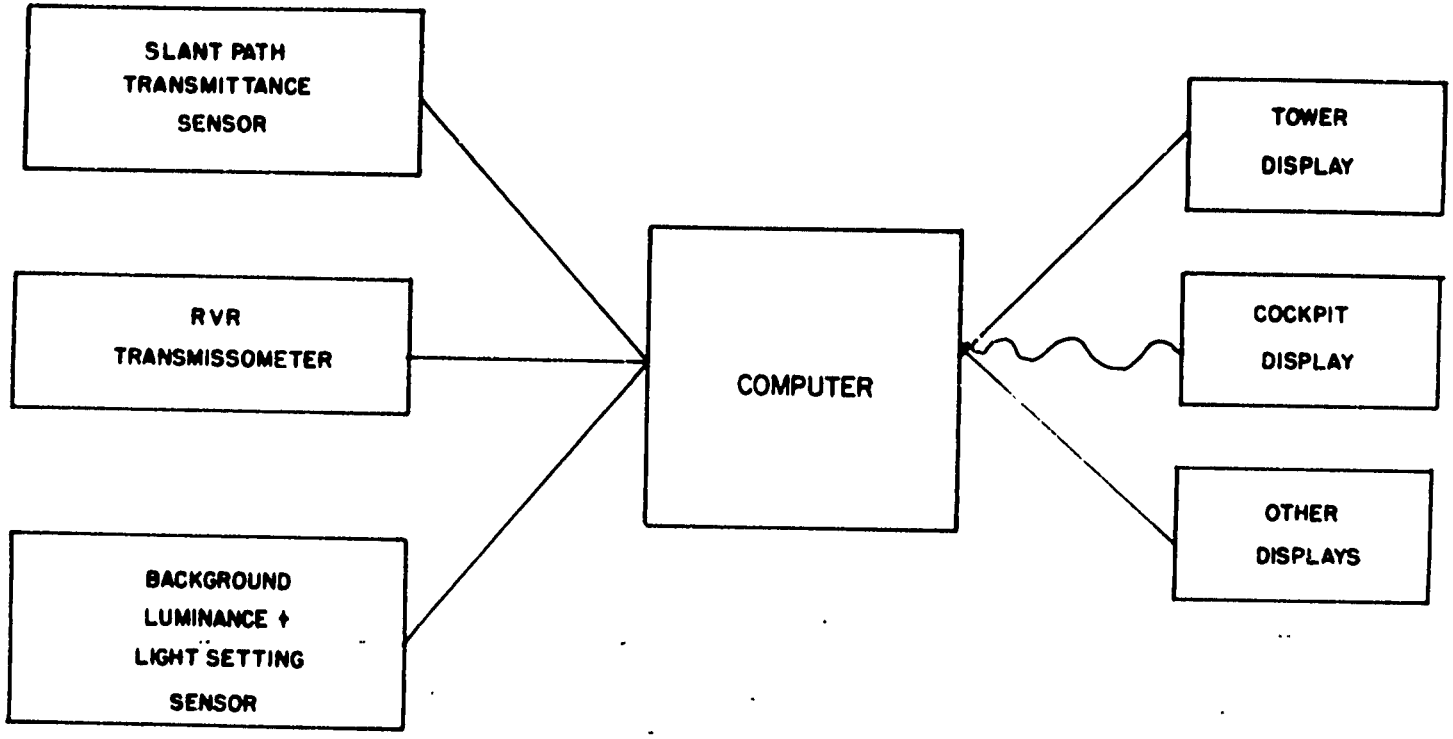

Figure 9. Basic Building Blocks of Future Visibility System

SOME REMOTE SENSING TECHNIQUES

Back Scatter Theory and the LIDAR Equation

In a previous section we discussed the meaning of visibility and its relation to atmospheric extinction of light. We will now concentrate on the basic principles involved in the remote sensing of the visibility. The difference between the conventional transmissometer and a remote sensing instrument is that the transmissometer is a dual ended device, restricted to measurements between the two "ends". A true remote sensor should be single ended. For this purpose we envision a transmitter-receiver combination which can perform measurements in remote regions not restricted to the transmitter-receiver location.

The most promising technique along this line is to employ similar principles as used in conventional radar. An optical radar or LIDAR (light detection and ranging) emits light signals, and obtains information about atmospheric conditions-at-a-distance from the backscattered return signal. We will now derive and discuss the basic Lidar equation as it is applicable to visibility measurements. Consider a transmitter sending a light signal at wavelength λ along a direction R. Let the beam spread of the radiation be θ_T, where the subscript T refers to the transmitter. Let P_λ (t) be the power at λ emitted by the transmitter at time t, then the flux density I_λ at a point R from the transmitter (neglecting atmospheric effects) is

$$I_\lambda = \frac{P_\lambda(R-ct)}{\pi(R\theta_T/2)^2} \text{ Watts/m}^2 \qquad (12)$$

For non-monochromatic light sources, we must integrate equation 12 over the spectral content of the source and both I_λ and P_λ are considered spectral densities. We have assumed a unit index of refraction for the propagation effect in (12). This

is sufficient for visible light in the atmosphere. The shape of the signal $P_\lambda(t)$ will be specified later, when we consider both pulses and modulated C.W.

In the atmosphere, the pulse does not propagate as indicated in (12) but would be attenuated. As we already discussed, in the visible part of the spectrum, the atmosphere acts predominately as a scatterer, and we may neglect absorption. As before, let us assume that the scattering constituent of type η has a total scattering cross-section for light of wavelength λ of $\sigma(\lambda,\eta)$. Let the local density of such scatterers at point r be $N(\eta,r)$. Then the extinction coefficient is also dependent on position

$$\gamma_\lambda(r) = \sum_\eta N(\eta,r)\sigma(\lambda,\eta) \tag{13}$$

and the intensity of light which reaches a point R from the transmitter becomes

$$I_\lambda(R,t) = \frac{P_\lambda(R-ct)}{\pi(R\theta_T/2)^2} e^{-\int_0^R dr\gamma_\lambda(r)} . \tag{14}$$

The exponential decay accounts for the scattering out of the beam all along the path from r = 0 to r = R.

For a completely homogeneous distribution of scatterers, the density N and hence γ_λ do not depend on position, and the integral in the exponent of (14) reduces to γR.

The region of atmosphere through which the transmitted light propagates is a cone with an apex angle θ_T at the transmitter. Consider a volume element consisting of a slice of thickness dR of this cone. The particles in this volume scatter light according to the differential scattering cross-section $d\sigma/d\Omega$. The light scattered into a solid angle element $d\Omega$ at angles θ, ϕ is proportional to the scatter coefficient β

$$\beta_\lambda(r,\theta,\phi) = \sum_\eta \frac{d\sigma}{d\Omega}(\lambda,\eta)N(\eta,r) \qquad (15)$$

where the summation over η has the same meaning as in Equation (4), and the density of scatterers of type η depends on the position. The general problem of how the scattered light further scatters is a complicated multiple scattering problem. Such questions are considered in detail in treatices on radiative transfer[12] in stellar and planetary atmospheres. For this report, we will restrict ourselves to the single scattering problem, realizing that in bad visibility (dense fog, etc.) the multiple scattering effects should be considered. Next we consider a receiver located at or near the transmitter. Let the receiver have a field of view characterized by a cone with apex angle θ_R. Under the assumption of single scattering, the receiver detects a backscattered signal from the transmitter only if the fields of view of the receiver and transmitter overlap. (This fact may be used to study the importance of multiple scattering.) This overlap is characterized by a common area $A_c(R)$ of the two intersecting cones as shown in Figure 10. The area is a distance R_1 from the transmitter, and R_2 from the receiver.

R_1 and R_2 may be equal, if the receiver is very close to the transmitter (a coaxial or bistatic configuration, for example) but this is not necessary.

The power scattered into the receiver at time t from the common volume element $A_c(R_1)\,dR_1$ is

$$dP_\lambda(t) = \beta_\lambda(R, \Theta_R, \Phi_R)\, d\Omega_R A_c(R_1) dR_1$$
$$\times \left[\frac{P_\lambda(ct-R_1-R_2)}{\pi(R_1\theta_T/2)^2} e^{-\int_o^{R_1} dr\gamma_\lambda(r)}\right] e^{-\int_o^{R_2} dr\gamma_\lambda(r)} \qquad (16)$$

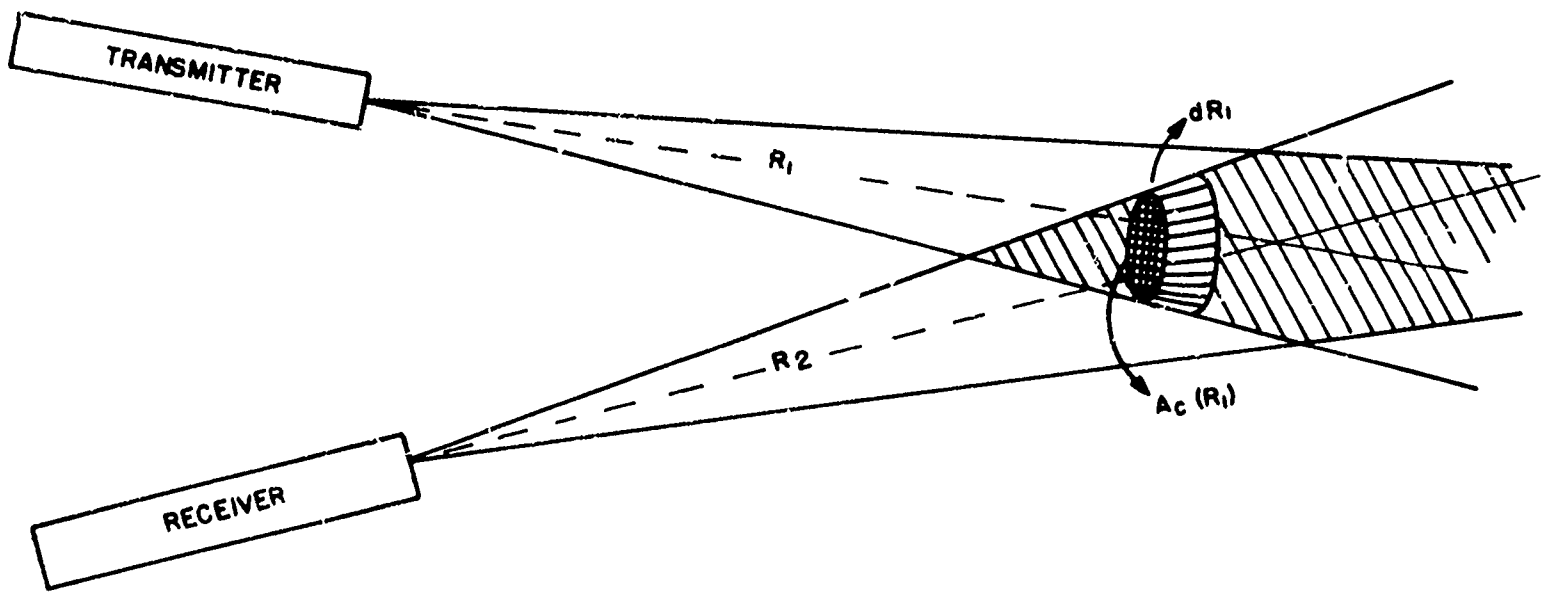

Figure 10. Receiver-Transmitter Geometry with Overlapping Fields of View Showing Common Volume Element

where $\beta(R_1,\Theta_R,\Phi_R)$ is the scatter coefficient at R_1 for scattering into the direction Θ, Φ of the receiver, $d\Omega_R$ is a solid angle element of the receiver collecting area subtented at R_1, the expression in the brackett is the intensity reaching R_1, and the final exponential accounts for the attenuation from the scattering volume to the receiver at R_2. Note that $R_2(R_1)$ is a function of R_1, and that the signal at time t at the receiver is delayed by $(R_1+R_2)/C$ with respect to the time when the signal $P_\lambda(t)$ left the transmitter. The total power received is obtained by integrating (16) over all R_1, and the total solid angle subtended by the collecting area of the receiver

$$P_\lambda(t) = \int_0^\infty dR_1 \int_{\Omega_R} d\Omega\ \beta_\lambda(R_1,\theta_R,\Phi_R)\, P_\lambda\ (ct-R_1-R_2)\ . \tag{17}$$

$$x\ \frac{A_c(R_1)}{\pi(R_1\theta_T/2)^2}\ e^{-\left(\int_0^{R_2} dr\gamma_\lambda(r)+\int_0^{R_1} dr\gamma_\lambda(r)\right)}$$

We have purposely been very general in our notation, so that we can analyze separately various assumptions which simplify the theory. Before going into those details, we note that the visibility is contained only in the extinction coefficient in the two exponents. To extract this information from the total return signal $P_\lambda(t)$ is no mean task. Some possible ways of accomplishing this will be discussed further on.

As it stands, Equation (17) is rather complicated. We will now investigate various simplifying assumptions with particular care to understand under what conditions they are valid. The simplifications may be grouped under three categories, receiver-transmitter geometry effects, outgoing signal considerations, and atmospheric model considerations.

1. RECEIVER-TRANSMITTER GEOMETRY

Equation (17) makes no assumption regarding the receiver-transmitter location. For Slant Visual Range measurements, we may for example envision the two systems shown in Figure 11. We assume that for both systems the receiver and transmitter field of view apex angles are small, (milli rads) and that the receiver collecting area A_R is small, so that the integral over the solid angle subtended by the receiver reduces simply to

$$\int_{\Omega_{Rec.}} d\Omega = \frac{A_R}{R_2^2} << 2\pi \qquad (18)$$

The angles θ_R and Φ_R become the angles between R_2 and the incident beam coordinate system. For a small separation d, the system shown in Figure 11 is a backscatter system. For relatively large separations between the receiver and transmitter in Figure 11, the system is a right angle scatter system. The backscatter system measures the extinction over the same path twice, once for the outgoing signal and once for the return. The right angle scatter system measures the extinction along two separate paths, R_1 and R_2. However, for a 3° glide slope, $R_1 >> R_2$, so that the extinction is measured predominately over the path of interest, R_1. To get a complete picture of the visibility with the right angle scattering system, either the receiver must scan through the transmitter beam or several receivers must be spaced along the ground. This complicates the system. For our present purposes we restrict ourselves to the backscatter system. The scattering function then becomes independent of the azimuthal angle Φ, and $\theta_R \approx \pi$, resulting in the notation

$$\beta_\lambda(R_1, \theta_R = \pi) \equiv \beta_\lambda(R_1) \qquad (19)$$

Equation 17 for a backscatter system becomes

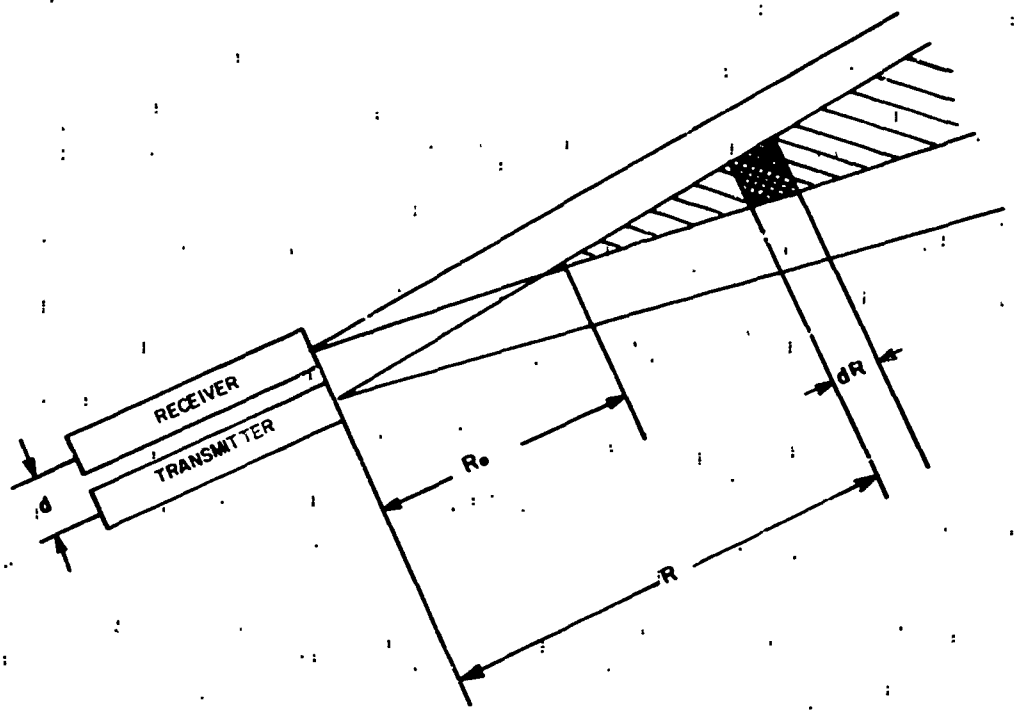

a) Nearly co-axial backscatter system

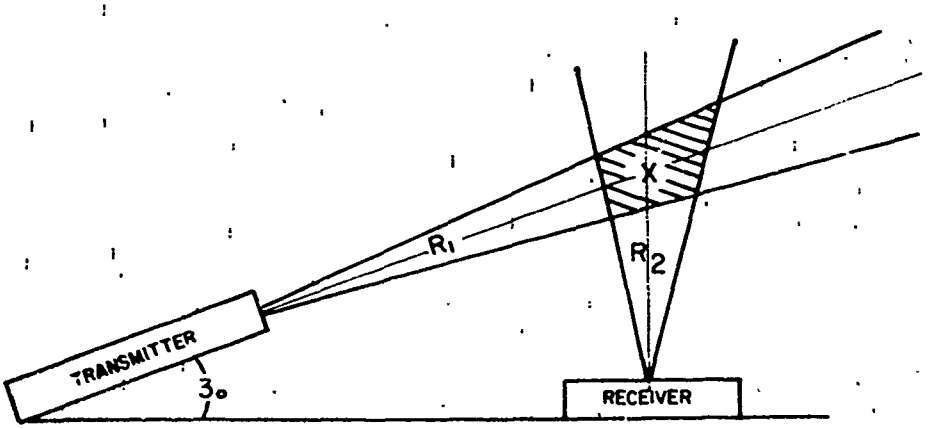

b) Side scatter system

Figure 11. Two Bistatic Lidar Systems

$$P_\lambda(t) = A_R \int_o^\infty \frac{dR\ A_c(R)}{\pi(R\theta_T/2)^2 R^2} \times \beta_\lambda(R) e^{-2\int_o^R \gamma_\lambda(r)\,dr} P_\lambda(ct-2R) \tag{20}$$

The detailed nature of $A_c(R)$ depends critically on the receiver-transmitter field of view geometry. We single out one particular example, where the receiver and transmitter have equal fields of view separated by a distance d. That is the case shown in Figure 11a. The two cones have equal apex angles, and their axes are parallel, but separated by a distance d. The common area $A_c(R)$ now becomes (Figure 12).

$$A_c(R) = \begin{cases} 0 \text{ ---- } R < R_o \\ 2(R \tan \theta/2)^2 \left[\cos^{-1}\frac{R_o}{R} - \frac{R_o}{R}\sqrt{1 - \frac{R_o^2}{R^2}}\right] \text{ ---- } R > R_o \\ \to \pi(R \tan \theta/2)^2 \text{ ---- as } R \to \infty \end{cases} \tag{21}$$

where $R_o = d/2 \cot \theta/2$

We note that $A_c(R)$ removes the apparent $1/R^4$ singularity in (20). In general, this singularity is unphysical. Its origin lies in the solid angle argument, Equation (18), and the beam spread argument, Equation (12. Neither of these two equations is valid near R = 0. Equation (12) is limited by diffraction effects, and Equation (18) by a maximum solid angle. Nevertheless, even though Equation (20) is not singular at R = 0, we will find that the strongest return signal comes from regions of space near the transmitter. Basically, there is a competition between the increasing common area $A_c(R)$ and the $1/R^4$ and exponential decrease. In general, the receiver-transmitter geometry contained in

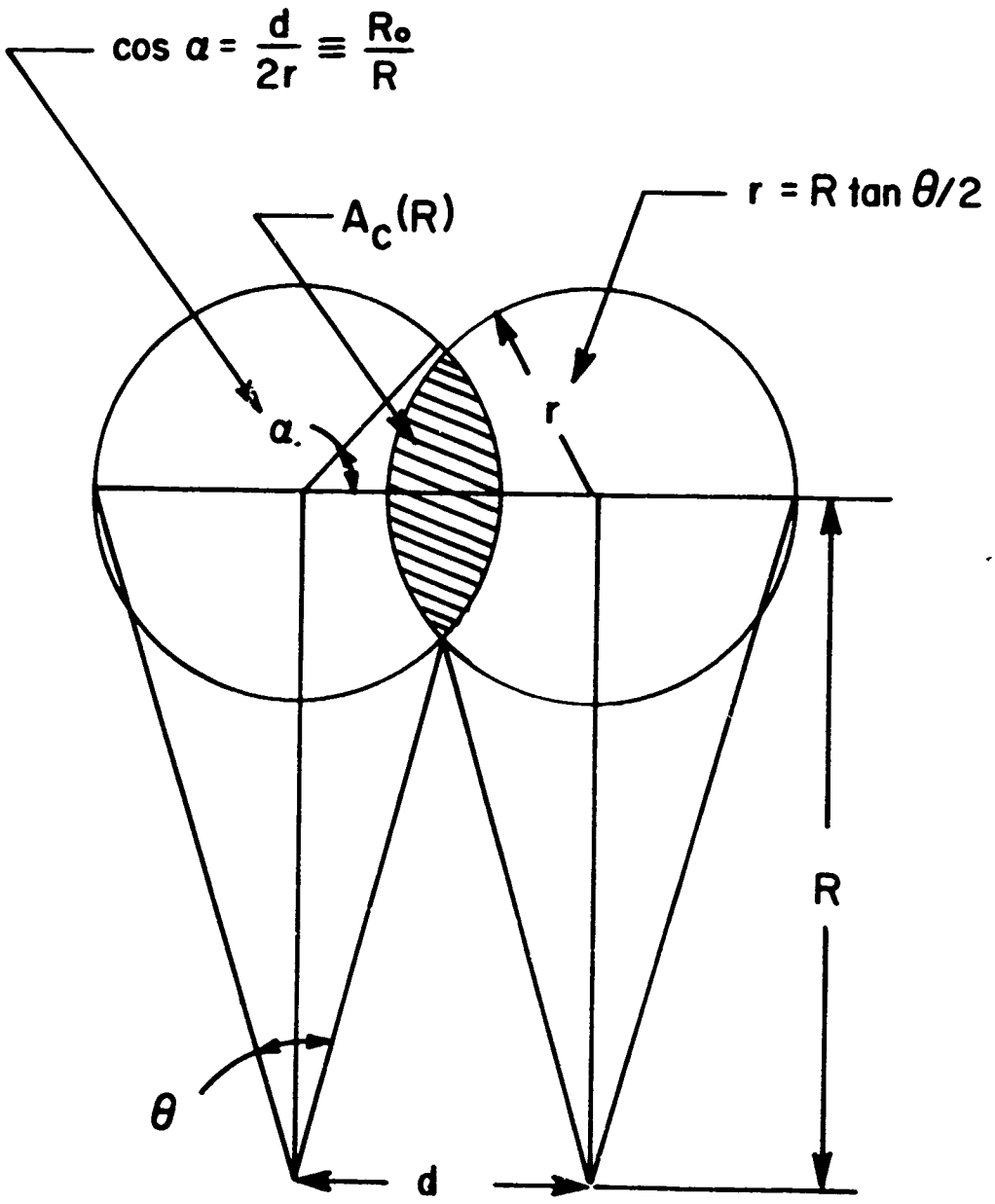

$$A_C(R) = 2(\alpha r^2 - r^2 \cos\alpha \sin\alpha)$$

Figure 12. Common area for Equal Field of View Case

Equation (17) causes no particular problem, and can be worked out for a specific system.

2. OUTGOING SIGNAL - SHORT PULSE

Further simplifications result if we restrict the outgoing light signal to a short pulse. Let us assume an outgoing rectangular pulse shape.

$$P_\lambda(t) = \begin{cases} P_\lambda^o & |t| \le T/2 \\ 0 & |t| > T/2 \end{cases} \tag{22}$$

where T is the full pulse width. If one substitutes this into Equation 20 for the backscattered return signal, the integral collapses to the range $|ct - 2R| \le CT/2$. If CT is smaller than any characteristic distance over which the integral in (20) (not including $P_\lambda(t)$ changes appreciably, the pulse $P_\lambda(t)$ behaves pretty much like a delta function, and the integral becomes

$$P_\lambda(t) = A_R \frac{cT}{2} \frac{A_c(R) P_\lambda^o}{\pi\left(\frac{R\theta_T}{2}\right)^2 R^2} \; x \tag{23}$$

$$\beta_\lambda(R) \; e^{-2\int_o^R \gamma_\lambda(r)\, dr}$$

where $R = ct/2$ to indicate that the return at time t after the pulse left the transmitter originated from the region at $R = ct/2$. We are still assuming a monochromatic light source, so the pulse length must include many optical cycles. Clearly, there is no problem to have short pulses compared to the scale of length over which atmospheric inhomogeneties occur, and yet, include many optical wavelengths. Pulsed laser are particularly suited for this purpose, as we will discuss in a later section.

If longer pulses, or C.W. signals are used, no particular simplification of Equation (20) results, and each case has to be

worked out separately. One such example using a modulated C.W. signal is discussed in detail in a later section. Again we remark, that for non-monochromatic light sources, the received power $P_\lambda(t)$ is a spectral density, and all relevant quantities have to be integrated over the spectral characteristics of the source.

3. ATMOSPHERIC CONDITIONS

Finally we turn to some simplifications which result from assumptions about the atmospheric conditions. Suppose the atmospheric conditions are homogeneous, that is, the density $N(\eta)$ of scatterers is independent of position. The short pulse lidar equation, (23) reduces to

$$P_\lambda(t) = \frac{cT}{2} \frac{A_R A_c(R)\ P_\lambda^o}{\pi\left(R\theta_T/2\right)^2 R^2} \beta_\lambda\ e^{-2\gamma_\lambda R} \tag{24}$$

again, $R = ct/2$. The shape of the return signal is now completely specified, and the visibility can be extracted from the exponential tail. This is in general not possible from equation (23).

The most serious problem in the whole backscatter (or sidescatter) theory comes from the fact that the atmospheric parameters enter the equations both in the β and γ. The visibility is determined only from the total extinction coefficient γ, but the magnitude of the return signal is directly proportional to β. One might expect that γ and β are related, since they are manifestations of the same physical process. This is basically correct, but the relationship is in general not very useful. From their definitions, we have

$$\beta_\lambda = \sum_\eta \frac{d\sigma}{d\Omega}(\lambda,\eta)\Big|_\pi N(\eta) \tag{25}$$

and

$$\gamma_\lambda = \sum_\eta \sigma(\lambda,\eta)N(\eta) \quad . \tag{26}$$

Only for the simplest scattering laws can one relate (25) and (26). For example, for an isotropic scatterer,

$$\frac{d\sigma}{d\Omega} = \frac{\sigma}{4\pi} \tag{27}$$

for all angles, and hence

$$\beta_\lambda = \frac{\gamma_\lambda}{4\pi} \tag{28}$$

Similarly, for Rayleigh scattering [13] of unpolarized light, the ratio of the total cross-section to the backward scatter cross-section is $8\pi/_3$, giving

$$\beta_\lambda = {}^{3\gamma_\lambda}/_{8\pi} \qquad \text{(Rayleigh)} \tag{29}$$

The more relevant example would be Mie scattering, but in this case no simple relationship like (28) or (29) results. The ratio of $d\sigma/d\Omega|\pi$ to σ depends on the droplet radius, and hence β/γ depends strongly on the distribution of the radii of the scatterers. Some examples along these lines have been calculated by Twomey and Howell,[14] who found a strong dependence on the size distribution. Further, for realistic atmospheric conditions, the variety of scatterers which occur, (snow, rain, haze, fog, industrial pollutants, etc.) is so large, that it would be practically impossible to compute the scattering cross-sections and distribution of parameters necessary to evaluate either γ_λ or β_λ. However, some empirical relationships between γ and β have been found by Curcio and Knestrick[15] from experimental data, and by Twomey and Howell[14] from model calculations. In both cases, non-monochromatic light was used, so that a spectral average for β_λ and γ_λ is involved. The general form of such a relationship in our notation is

$$\beta = K_1 \gamma^{K_2} \tag{30}$$

where K_1 and K_2 are constants. The crucial constant K_2 is typically 1.5. Since in general, there is no theoretical justification of a relationship like (30), it is advisable to concentrate on signal processing techniques which can extract γ from the backscattered signal without any reference to β.

A final point should be mentioned. There has been some discussion about the relative merits of using white light vs. monochromatic light for the backscatter technique.[15] Since Mie scattering contains only the parameter (λ/a), where a is the particle size, an integration over the spectral characteristic of the light source has a similar effect as the integration over particle sizes. This averaging further smoothes out irregularities in β_λ and γ_λ, and is advantageous, especially for empirical relationships. This was the conclusion of Twomey and Howell.[14] Unfortunately, white light sources have other disadvantages which make monochromatic sources (lasers) more attractive for backscatter work, since short pulses are readily available.

Signal Processing

In this section we briefly indicate how the visibility can be extracted from the return pulses of a pulsed lidar. To begin with, let us restrict ourselves to homogeneous atmospheric conditions, so that Equation (24) is applicable. The shape of the return signal, as seen on our oscilloscope for example, is completely determined by replacing all R by $ct/_2$ on the right of Equation 24, so that

$$P_\lambda(t) = C\beta_\lambda \frac{A_c(t)}{t^4} e^{-\gamma_\lambda ct} \tag{31}$$

where all constants have been lumped together into C. As discussed in the last section, there is no singularity,

$A_c(t)/_t 4 \to 0$ as $t \to 0$. To show how the return signal $P_\lambda(t)$ depends on the visibility, we plot Equation (31), or $P_\lambda(t)$ as a function of t and $R = ct/_2$ for various values of the visibility. Since $P_\lambda(t)$ is proportional to β_λ, we have to assume a particular model of β vs γ to be able to compare returns from different visibilities. For simplicity, we take the case of isotropic scattering, Equation (21). For the receiver-transmitter geometry we take the biaxial system described previously, so that the results leading to $A_c(R)$, Equation (21), are applicable. The computations were performed with the following parameters:

$d = 50$ cm.

$\theta = 10$ mili radians,

leading to the closest return distance $R_o = 50$ meters, or 1/ of a microsecond from the time the outgoing pulse left. The are shown on Figure 13, where the relative amplitudes of under five different visibility conditions are plotted as a function of the range of the return and the time of the return. These curves show the following characteristics. The return signal begins at $R_o = 50$ m where the receiver-transmitter fields of view begin to overlap. This overlap increases and competes with the $1/_R 4$ and exponential $e^{-\gamma R}$ decrease of the signal, resulting in a maximum, after which the $1/_R 4\ e^{-\gamma R}$ dominates. The relative amplitudes, particularly the maxima, have an interesting dependence on the visibility. Since $P_\lambda(t) \sim \beta_\lambda \sim 1/V$, the amplitudes of the lower visibility returns are expected to be higher. However, for low visibility, the exponential decay is faster, so that we again have two competing effects. The maxima of the return signals increase as the visibility decreases from 2 km to .5 km, but then decrease as we go to .2 km and .1 km visibility. The location of the range from which maximum return originates (or the time of the peak) also increases with visibility, but at a very slow rate. These results would indicate how to extract the visibility from the

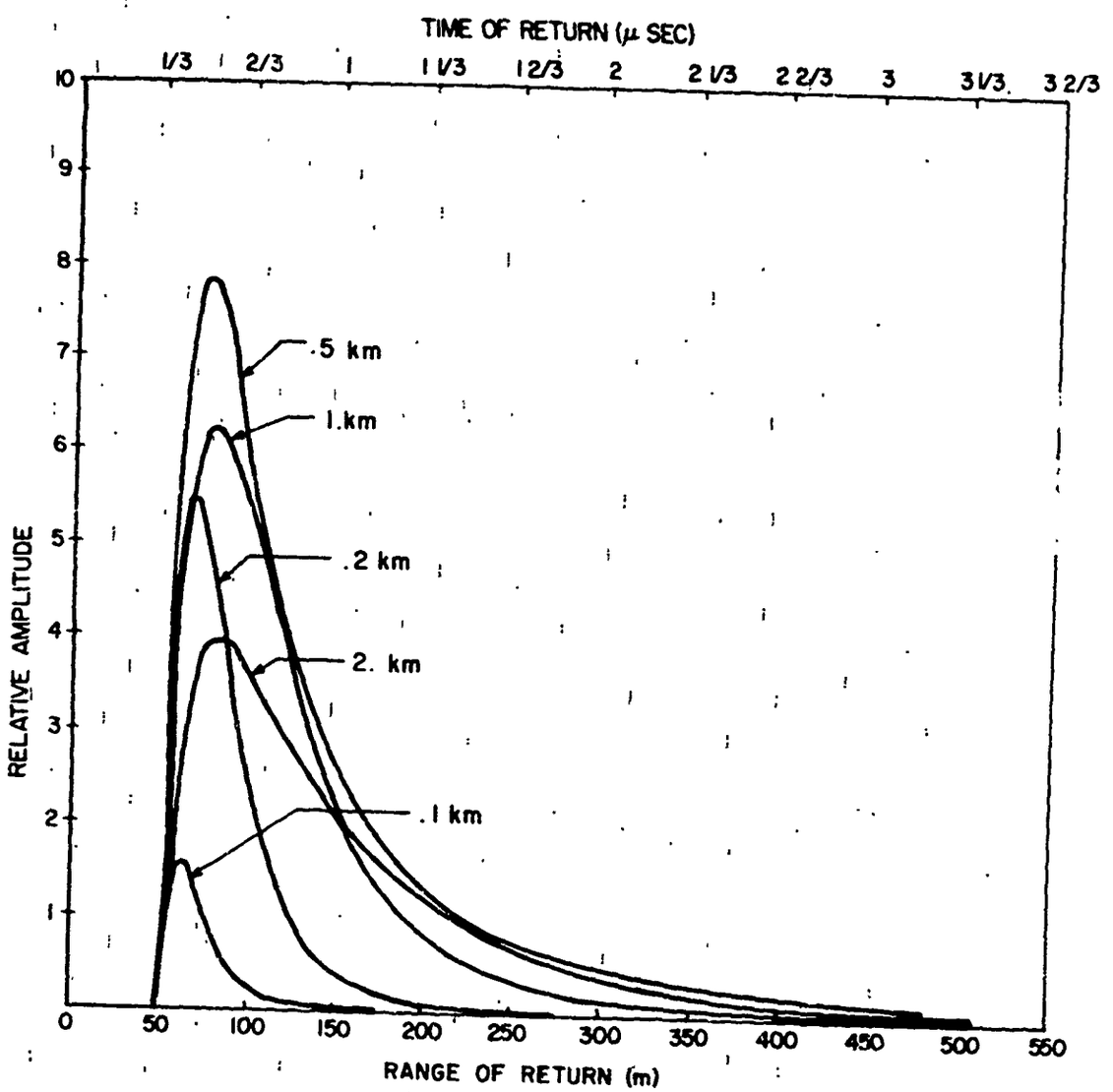

Figure 13. Return Signals (Relative Amplitude) from Visibility of .1 Km, .2 Km, .5 Km, 1 Km and 2 Km as a function of the Time of Return (μsec) and Range (m) of Return

return signals. However, the results mentioned so far depend very strongly on the example considered, both from the γ vs β model point of view and the receiver-transmitter geometry. This complicates matters considerably. Brown[16] has shown that the width of the return pulse may be a better criterion, however, it too is not free from the above objections.

A further objection arises if we consider non-homogeneous atmospheric conditions. The above model is not applicable, and the return pulses could be distorted from the ones shown on Figure 13.

A technique to circumvent some of these difficulties was developed by T. H. Collis[17] and his group at the Stanford Research Institute. Their basic idea consists of eliminating the known time dependence of the return signal, the $1/t^4$ and $A_c(t)$ effect and analyzing the left over range corrected signal

$$\beta_\lambda(R)\, e^{-2\int_0^R \gamma_\lambda(r)\, dr}.$$

This technique still requires some assumptions about $\beta_\lambda(R)$, but looks more promising. In particular, it may have the possibility of obtaining a local value of the visibility, or $\gamma_\lambda(R)$.

It appears that more analytical and experimental work on the backscatter technique has to be performed before a reliable interpretation of the results is obtained. Because the variety of atmospheric phenomena is so large and complex, it may be necessary to use other meteorological data in conjunction with the backscattered signal to obtain a measure of the visibility. This requires that further backscatter experimentation be carefully correlated with other prevailing meteorological data.

Possible Pulsed LIDAR Systems

In this section we discuss some systems which might be suitable for carrying out the measurements discussed in the previous sections. By systems, in this context, we mean simply a transmitter of sufficient power and receiver-detector of sufficient gain to detect the backscattered signal. Eye-safety considerations will be discussed in the next section.

To carry out the calculations implied above, we must estimate the magnitude of the return signals. The considerations of the previous section, which led to the relative backscatter signals will again be applied, but we must now include all the parameters which appear in Equation (24) to get an estimate of the magnitudes involved. As we mentioned in the last section, it is not yet clear what characteristics of the return pulse are best suited for computing the visibility. However, it is clear that the overall pulse slope is involved. With this in mind, the requirement that the peak of the pulse can be detected with a signal-to-noise ratio of about 20 within an appropriate bandwidth seems a reasonable criterion for estimation purposes. From Figure 13 we note that the maxima of the return pulses occurs at about 75 meters. (Note that this is only true for the particular lidar configuration.) The peak return power is then obtained by substituting R_{max} = 75 m into Equation (24).

$$P_\lambda(t_{peak}) = (.1)\ \frac{CT}{2}\ \beta_\lambda\ \frac{e^{-2\gamma_\lambda R_{max}}}{R_{max}^2}\ P_\lambda^o A_R \qquad (32)$$

The ratio $A_c\ (R_{max})/(R_{max}\ \theta/2)^2\pi \simeq .1$ was computed from Equation (23). For the example we are investigating, the smallest return signal occurs for the 100 meter visibility case. From the visibility-γ relation, Equation (2), and the β-γ relation, Equation (28), one finds

$$P_\lambda(t_{peak}) = .02\ A_R\ T\ P_\lambda^o \text{ watts}, \qquad (33)$$

where A_R is the collecting area (m^2) of the receiver, T the pulse length and P_λ^o the power of the outgoing pulse. We note the important result that P_λ is proportional to TP_λ^o or the total energy of the outgoing pulse.

The dominant source of noise which has to be considered for a visibility measuring device is due to background radiance. The receiver might be looking at a bright cloud or fog with a spectral radiance of $N(\lambda)$ watts per cm^2 x Å x steradian. The total background power received is

$$P_B^\lambda = N(\lambda) A_R \Delta\lambda \pi \left(\frac{\theta}{2}\right)^2, \tag{34}$$

where the only new quantity introduced is the spectral width of the pre-detection optical filter, $\Delta\lambda$. This background power is not the noise, since it could be subtracted from the signal. The noise arises from the fluctuations produced by the background in the typical detector, and as such, competes with the fluctuations produced by the signal itself.

Such considerations then depend on the type of detector used. A graph showing the diffuse component of the typical background radiance at sea level is shown in Pratt's[18] book. The radiance from sunlit clouds or fog is about an order of magnitude larger. We now apply these considerations to some typical pulsed systems.

1. RUBY LASER - PHOTO-MULTIPLIER DETECTOR.

The ruby laser operates at a wave length $\lambda_1 = 6943$Å and the energy per pulse, TP_λ^o can easily be as much as 1 joule. The pulse length should be shorter than typical distances over which the integrand is the lidar equation (20) changes. Roughly, this requires $c\tau < V_{is}$. For a 100 meter V_{is}, this requires $T < 300$ nanoseconds which is no problem.

For the detector we specify a S-20 photomultiplier with a cathode sensitivity η of about 20 mA/Watt and a gain g of 8×10^6.

The signal current from such a device is:

$$I_{sig} = g\eta P_{\lambda_1} \tag{35}$$

and the noise current is

$$I_{noise} = g\sqrt{2e\Delta f\eta\left(P_B^{\lambda}+P_{\lambda_1}\right)} \tag{36}$$

where e is the charge of the electron, and Δf the post detection bandwidth required to resolve the return pulse. At this point we must be careful not to confuse the outgoing and return pulse width. The outgoing signal pulse must be short, in particular, it was assumed to be a δ function with a given energy TP_o^{λ}. The return pulse width is determined by the visibility and configuration of the lidar, and is independent of the width of the outgoing short pulse. For this reason, Δf should not be taken inversely propagational to T. Judging from the return pulses shown in Figure 13, the pulse width of the narrowest return (.1 km V_{is}) is about 30 meters. Hence, we take

$$\Delta f = \frac{2\pi}{T_{ret}} \approx 100 \text{ MHz} \tag{37}$$

The current signal to noise ratio becomes

$$I_{sig}/I_{noise} = \eta P_{\lambda_1}/\sqrt{2e\Delta f\eta\left(P_B^{\lambda} +P_{\lambda_1}\right)} \tag{38}$$

and is signal or background noise limited depending whether P_{λ_1} or $P_B^{\lambda 1}$ predominates in the denominator.

For the spectral radiance at the ruby laser wavelength we take $10\mu W/cm^2A$. This is about 20 times the diffuse clear sky background in Pratt[18], which should correct for the increase due to sunlit clouds or fog. For our 10 mil. rad. system, with a $\Delta\lambda = 20$ Å optical filter, the background power becomes $P_B^{\lambda 1} = 2 \times 10^{-4} A_R$ watts, where A_R is the area (m^2) of the collecting optics.

Substituting these results in to Equation (38), we find

$$\frac{I_{sig}}{I_{noise}} = \frac{500\ T P^{o}_{\lambda_1} \sqrt{A_R}}{\sqrt{.02\ T P^{o}_{\lambda_1} + 2 \times 10^{-4}}} \quad . \qquad (39a)$$

2. NEODYMIUM LASER - PHOTOMULTIPLIER

A typical neodymium glass laser lases at $\lambda_2 = 1.06\mu$, which is best suited for a S-1 photomultiplier detector. The same analysis as for the ruby system applies. The photomultiplier characteristics are a cathode sensitivity of about .4mA/W and a gain of 10^6.

The spectral radiance from the background at the neodymium wave length is about a factor of 20 lower than for ruby, so that the signal to noise current ratio becomes:

$$\left.\frac{I_{sig}}{I_{noise}}\right|_{Nd.} = \frac{70\ T\ P^{o}_{\lambda} \sqrt{A_R}}{\sqrt{.02\ T\ P^{o}_{\lambda} + 1 \times 10^{-5}}} \quad . \qquad (39b)$$

This estimate assumes that there is no significant change in the extinction and backscatter coefficient as we go from λ = 6043 to 10630 Å.

3. GALLIUM ARSENIDE LASER - PHOTOMULTIPLIER.

The gallium arsenide laser lases at about λ_3 = 8600 Å. GaAs photomultipliers with a cathode sensitivity of 30mA/Watt in this spectral range are available.

The spectral radiance from the background in the 8600 Å region is about a factor of 5 lower than for ruby. The signal to noise current ratio now becomes

$$\left.\frac{I_{sig}}{I_{noise}}\right|_{GaAs} = \frac{600\, T\, P^{o}_{\lambda_3}\sqrt{A_R}}{\sqrt{.02\, T\, P^{o}_{\lambda_3} + 4 \times 10^{-5}}} \quad . \qquad (39c)$$

Again we have assumed that the backscatter signal does not differ from that of the ruby case.

To compare the three systems discussed above, we plot the results of Equations (39a - 39c). Since the relevant variables in these equations are the total energy $E = TP^{o}_{\lambda}$ per pulse emitted by the transmitter and the area normalized signal to noise ratio, we plot $I_{sig}/I_{noise}\sqrt{A_R} = \rho$ vs E. The general form of Equations (39a - 39b) then becomes

$$\rho = \frac{aE}{\sqrt{bE+c}}, \qquad (40)$$

where a, b, c are readily identified from (39a - 39c). These results are shown in Figure 14.

The graph shows that for the system parameters chosen, GaAs seems the most suitable, followed by Ruby, and then Nd. Since eye safety aspects play an important role in operating any laser system in a non-restricted environment, we have indicated along the top of the graph an abcissa listing the cross sectional area of the outgoing beam which makes the particular energy per pulse eye safe. Since we are dealing with short pulses (<1μsec.) we find from Appendix II that the medium conservative estimate requires an intensity of less than 10^{-7} joules/cm^2 per pulse. Hence, for higher pulse energies, the area must be scaled up.

Reading the graph is simple. For example, suppose a signal to noise (I_{sig}/I_{noise}) ratio of 20 is required for signal processing a pulsed ruby return. If we plan to use a collector area of 200 cm^2 (about 6" diameter), $\rho = 20/\sqrt{.02} = 140$ m^{-1}, we need about 5×10^{-3} joules per pulse, which requires an eye safe beam area of about 5m^2. With the 10m rad. beam divergence, the

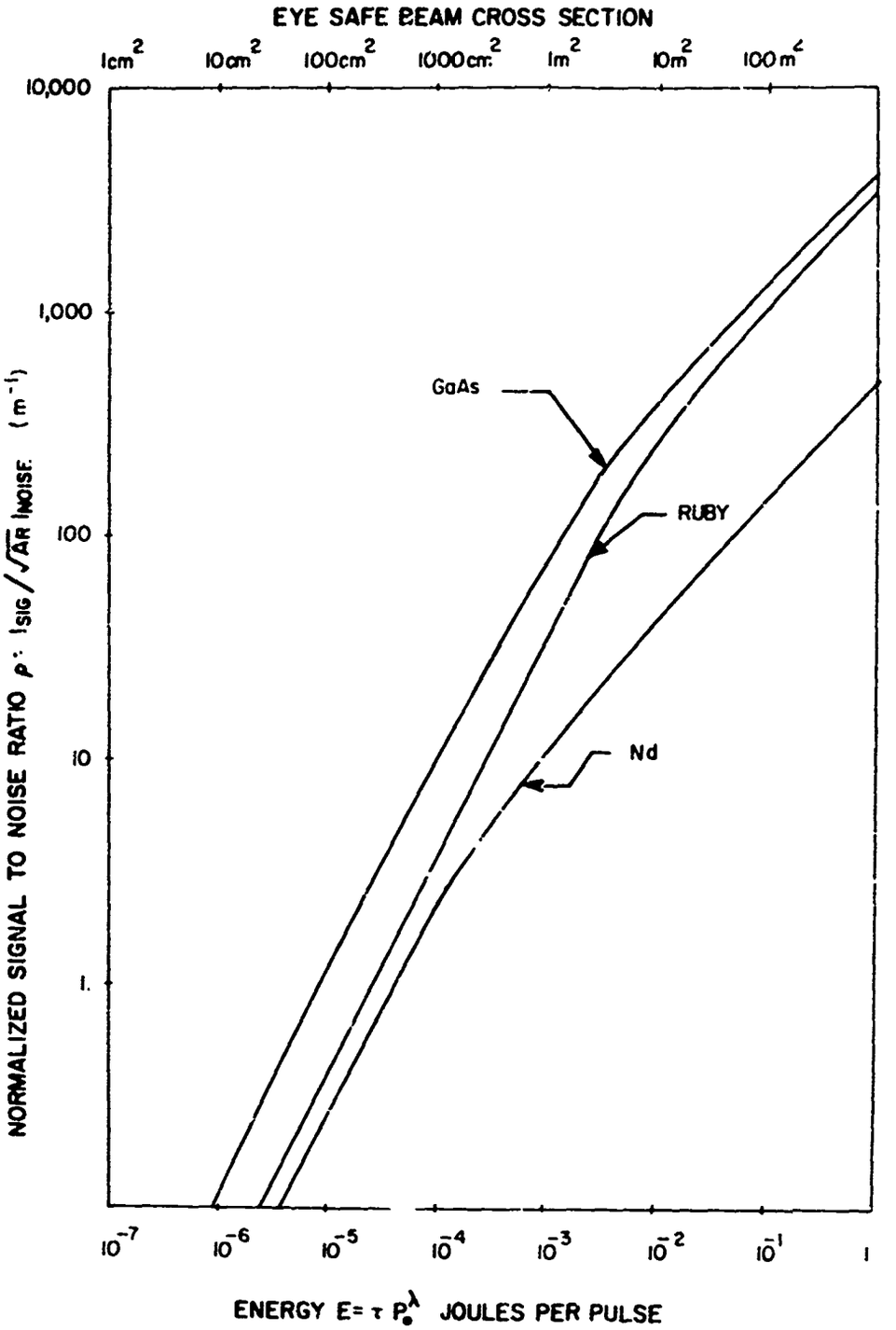

Figure 14. Receiver Area Normalized Signal to Noise Ratio vs Energy Per Pulse for GaAs, Ruby, and Nd Pulsed Lidar System (For Each Energy Per Pulse, there is a Beam Cross Sectional Area for which the Pulse is Eye Safe. This Area is Indicated on the Top of the Figure.)

beam would be eye safe at distances of about 500m from the transmitter, unless the outgoing beam is optically expanded to $5m^2$ at the transmitter. For GaAs we would require about a factor of 2 less energy, for Nd a factor of 10 more for the same system. The analysis presented in this section is not be to considered complete. We have analyzed a particular system configuration for three different transmitter-receiver combinations and compared them on an equal energy per pulse basis. The other factor which enters the analysis is the pulse rate capability of the system. The larger the number of pulses per second, the better the statistics which can be achieved for a given type of signal processing. A ruby laser can be pulsed at least a few times per sec. without possible damage to the rod. Nd/Yag and GaAs on the other hand can be operated at pulse rates of 10-100 pps. and 10^3 or so pps. respectively. The energy per pulse is then primarily determined from eye safety considerations, and the pulse rate is determined from the signal processing requirements.

Modulated C.W. System

Consider a typical HeNe laser (6328Å) followed by an electro-optic modulator. The intensity of the light after the modulator is

$$I_{out} = I_{in} \sin^2 \pi\delta \tag{41}$$

where $\pi\delta$ is the retardation induced by the modulator. Let

$$\pi\delta = \alpha + \frac{\pi}{2} \frac{V}{V_{1/2}} \sin \omega t \tag{42}$$

where α is a constant retardation, obtained by either a dc bias voltage on the modulator or an optical retardation, V and ω are the voltage and frequency of the modulation signal and $V_{1/2}$ is the 1/2 wave voltage characteristic of the modulator crystal. The outgoing intensity may be expanded in the form

$$I_{out}/I_{in} = \frac{1}{2}\left\{1 - \cos 2\alpha\left[J_o\left(\frac{\pi V}{V_{1/2}}\right) + 2\sum_{n=1}^{\infty} J_{2n}\left(\frac{\pi V}{V_{1/2}}\right)\cos 2n\omega t\right]\right.$$

$$\left. + \sin 2\alpha\left[2\sum_{n=0}^{\infty} J_{2n+1}\left(\frac{\pi V}{V_{1/2}}\right)\sin (2n+1)\ \omega t\right]\right\} \qquad (43)$$

which specifies the harmonics in the intensity in terms of ordinary Bessel functions. Usually, one requires that the modulator produces only the first harmonic and hence a bias of $\alpha = \frac{\pi}{4}$ is used. The voltage V then determines the modulation depth and harmonic distortion, (3rd and higher odd harmonics).

For our purposes, we leave the choice of α and V open, since we may want to take advantage of the harmonics furnished by the crystal. To simplify the discussion, we express the nth harmonic of the light intensity emerging from the modulator in the form

$$I_{out}^{n} = I_n \begin{cases} \sin n\omega t & n = \text{odd} \\ \cos n\omega t & n = \text{even} \end{cases} \qquad (44)$$

where the amplitude I_n is readily identified from (43). The instantaneous harmonic intensity in space, confined to the cone defined by the laser-modulator beam divergence is then

$$I_{out}^{n} = I_n \begin{cases} \sin n\omega(t - \frac{R}{c}) & n = \text{odd} \\ \cos n\omega(t - \frac{R}{c}) & n = \text{even} \end{cases} \qquad (45)$$

where R is measured along the axis of the cone; R = 0 is the apex at the laser-modulator transmitter system. The actual beam profile is not important for the following discussion. The index of refraction of the atmosphere is unity for our purposes.

Consider a detector located near or at the transmitter. The field of view of the detector and the cone of the transmitted signal overlap, hence there is backscattering into the detector. The total backscattered power received is derived by going through the same arguments as required for the derivation of the pulsed lidar equation. We restrict ourselves to a homogeneous atmosphere.

Let

$$\frac{A_c(R)}{\pi\left(\frac{R\theta_T}{2}\right)^2} = f(z) \rightarrow \begin{cases} 0, & R = 0 \\ 1, & R \rightarrow \infty \end{cases} \tag{46}$$

The zero at R = 0 is to be sufficiently strong to remove the unphysical singularity in the backscatter equation; the field of view of the detector completely overlaps the outgoing laser beam at a certain distance.

We now substitute our modulated outgoing signal into the backscatter equation. Using the Fourier decomposition (45) in Equation (20) we obtain the nth harmonic in the backscattered signal power at the detector.

$$P_n(t) = A_R \int_0^\infty dR\beta f(R) \frac{e^{-2\gamma R}}{R^2} P_n \times \begin{cases} \sin n\omega\left(t - \frac{2R}{c}\right) & n = \text{odd} \\ \cos n\omega\left(t - \frac{2R}{c}\right) & n = \text{even} \end{cases} \tag{47}$$

where we changed to total power P_n rather than intensity I_n. This signal may be written in the form

$$P_n(t) = A_R P_n \begin{cases} A_n(\omega)\sin n\omega t - B_n(\omega)\cos n\omega t \\ A_n(\omega)\cos n\omega t + B_n(\omega)\sin n\omega t \end{cases} \tag{48}$$

where

$$A_n(\omega) = \beta \int_0^\infty dz\ f(z)\ \frac{e}{z^2}^{-2\gamma z}\ \cos\ 2n\ \frac{\omega z}{c} \tag{49}$$

and

$$B_n(\omega) = \beta \int_0^\infty dz\ f(z)\ \frac{e}{z^2}^{-2\gamma z}\ \sin\ 2n\ \frac{\omega z}{c} \tag{50}$$

As far as the detector is concerned, the signal becomes

$$P_n(t) = A_R P_n \sqrt{A_n^2 + B_n^2} \begin{cases} \sin\ (n\omega t - \phi_n) \\ \cos\ (n\omega t - \phi_n) \end{cases} \tag{51}$$

where the phase

$$\phi_n = \tan^{-1} \frac{B_n}{A_n} \tag{52}$$

is relative to the power leaving the modulator at time t.

The visibility information, or γ, is now contained in the phase and amplitude of the return signal. Since B_n/A_n is independent of β, a phase measurement is not subject to any β vs γ model. The quantity $\sqrt{A_n^2 + B_n^2}$ may be called the normalized backscatter power (watts received/watts transmitted x receiver area) at the nth multiple of the fundamental modulation frequency. This power is proportional to β; however, the ratio of two backscattered signals at different modulation frequencies is again independent of β. To estimate the magnitudes of ϕ_n and $\sqrt{A_n^2 + B_n^2}$ and their dependence on the modulation wavelength and visibility, we have to use some model to be able to perform the integrations (49) and (50).

To simulate the receiver/transmitter geometry effect described by f(z) we use $f(z) = (\tanh \kappa z)^3$ in the integration. With $\kappa = .1$ meter^{-1} the overlap between the laser beam and

receiver field of view is 90% after about 20 meters. To estimate the magnitude of A_n and B_n, we use $\beta = \gamma/4\pi$ corresponding to isotropic scattering. We wish to emphasize again that this assumption is only necessary to estimate the strength of the return signal. The visibility, or γ, can be determined from ratios independent of β.

Figure (15) shows a plot of the magnitudes of $\sqrt{A_1^2 + B_1^2}\ m^{-2}$ as a function of the modulation wavelength for visibilities of 100, 200, 500, and 1000 meters. Figure (16) shows a plot of the relative phase ϕ_1 as a function of the visibility for modulation wavelengths of 50, 75, 100, 300 and 1000 meters. In both graphs we have used the definition (2) to relate visibility to the extinction coefficient. We note that both the backscattered power and phase show a marked dependence on the visibility. What is the best way of extracting the visibility or γ, keeping in mind that we do not want to make use of the magnitude of $\sqrt{A^2 + B^2}$ because of the β problem? Several methods come to mind. We note from Figure 15 that the slope of the backscattered power vs modulation wavelength has a strong dependence on the visibility. In the linear region between λ = 25m and 50m, a slope measurement is easily performed by taking the ratio of two return signals at different modulation wavelength. As we discussed in the beginning of this section, the modulator, if properly biased and driven, furnishes us with various harmonics. This may be used to advantage, for example we could get equal power output at 25 and 50m to perform the above slope measurement. Similarly, by performing phase measurements, the visibility is easily determined. For example, to cover the visibility range 0 to 200 meters (important for CAT III Aircraft Landing) the 75m modulation wavelength of our example system would give very good resolution. One might again work at more than one wavelength or make use of the discontinuity in the phase.

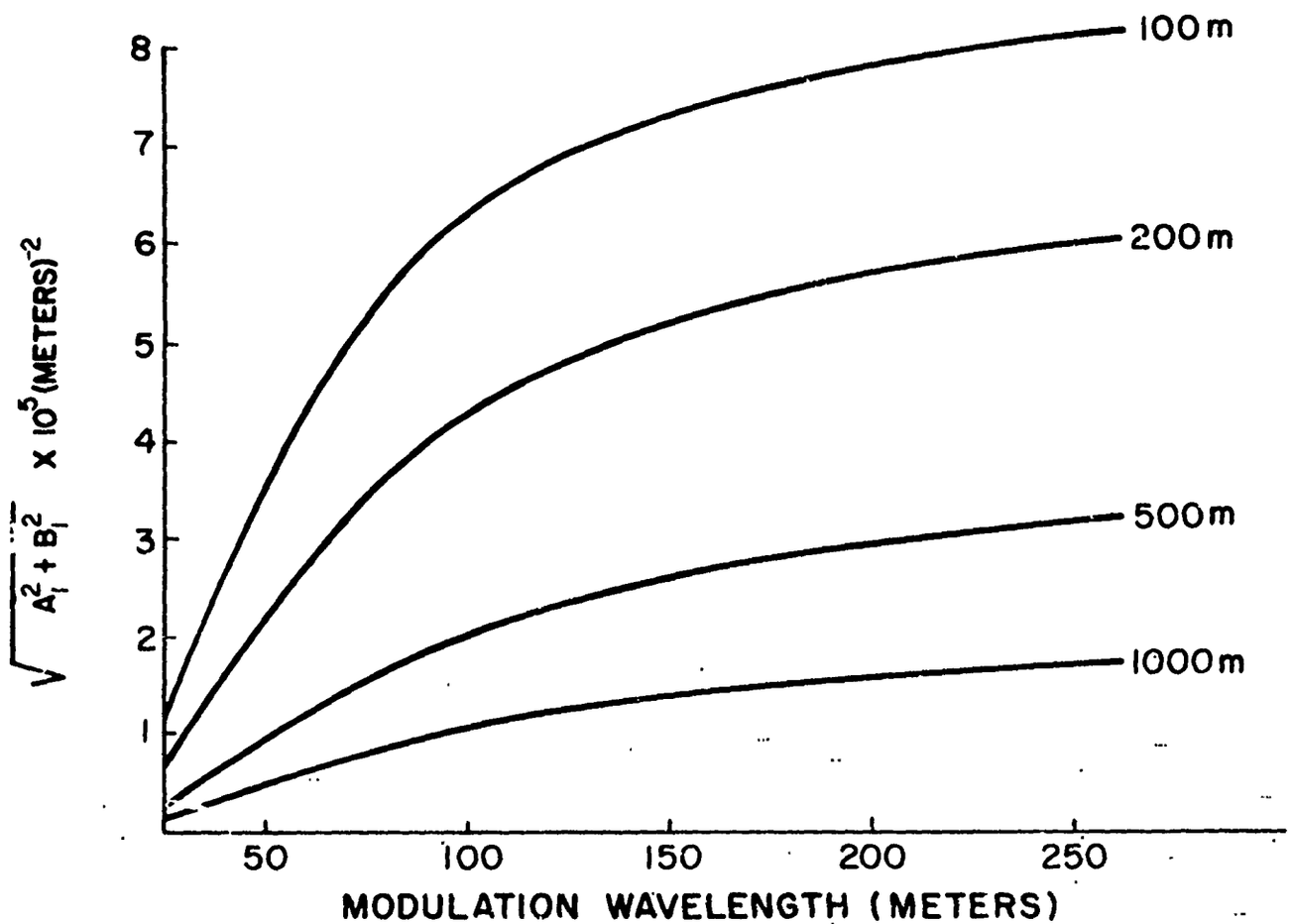

Figure 15. Normalized Backscattered Power $\sqrt{A^2 + B^2}(m^{-2})$ as a Function of the Modulation Wavelength (m) for 100, 200, 500 and 1000 Meter Visibility.

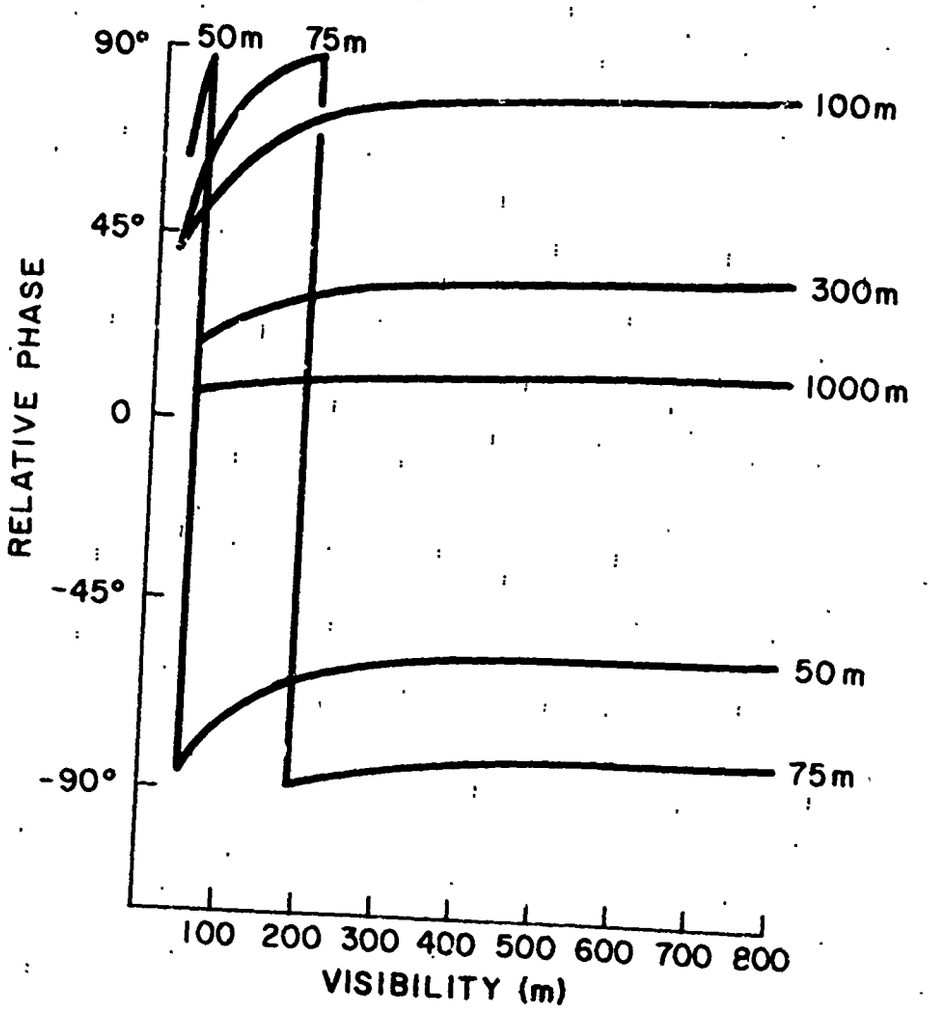

Figure 16. Relative Phase of the Backscattered Intensity as a Function of the Visibility (Meters) for Modulation Wavelength of 50, 75, 100 and 300 Meters.

The best way of extracting visibility information from the return signal will have to be determined from some experimentation. However, all the electronic signal processing will be in the megacycle range. The modulation frequency can be very sharp, which implies a narrow post-optical-detector bandwidth can be used. This is advantageous from the signal-to-noise point of view.

To get a feeling for the magnitudes of the quantities involved, we put a few numbers into our estimate for the power in the return signal. Form (51) we need $A_R P_n \sqrt{A_n^2 + B_n^2}$ which we estimate (for n = 1) as follows.

1. For the collecting area A_R of the detector we take $A_R \approx 100 cm^2$.
2. The transmitted modulated power is estimated from (43). We are interested in the fundamental P_1. Let the modulator be biased at 45° retardation and operated with a driving voltage (p-p) of about 1/2 of half wave voltage at a modulation wavelength of 100 meters, (3 MHz). P_1 is then about one half of the output of the C.W. Laser.
3. From the graph in Figure 15, the normalized backscatter power $\sqrt{A_1^2 + B_1^2}$ at 100m modulation wavelength and 500m visibility is about $2 \times 10^{-5} m^{-2}$.

The backscattered intensity for a 10mW HeNe laser, modulated at 3 MHz is then about 10^{-9}W. For a typical S-20 photomultiplier with a cathode sensitivity of η = 30mA/W and a gain g of about 8×10^6, we get a signal current of about .2 mA at 3 MHz.

The dominant source of noise such a system would encounter is due to background radiance. The receiver might be looking at a bright cloud or fog bank. To be pessimistic, we take a spectral radiance of 50$\mu W/cm^2$, Å, St. Rad. For a 1 mrad. field of view and 20 Å optical filter, this results in $10^{-9} W/cm^2$ back-

ground power density. The noise current produced by this background into our PMT is

$$I_{noise} = g\sqrt{2e\Delta f P_B \eta}$$

where P_B is the total background power collected, e the electronic charge and Δf the post-detection bandwidth. For the system parameters chosen above, and a Δf of 100 cycles, the background noise current becomes about 3.6μA. The dark current is much smaller. We conclude that there should be no signal-to-noise difficulties.

From the eye safety discussion in Appendix II, we note that to make a 10mW C.W. beam eye safe, we have to expand the beam until its intensity is 10^{-5} watts/cm^2 or less. Starting with a 1 mm radius beam at 10mW, we need to expand the outgoing beam by about a factor of 30 to 3 cm radius.

CONCLUSION

To conclude this report we summarize the specific points which deserve further attention.

1. The question whether two threshold illuminance E_T values suffice for all background brightness conditions should be reexamined. To chose more E_T steps is the recommendation of ICAO, but to continuously monitor the background luminance and derive the appropriate E_T values would not involve a more significant complication. Such a recommendation does not only apply to the present RVR system, but should be seriously considered in any future system. From the large spread of possible background luminances, it is precisely the unusual background luminance condition which deserves the most attention.

2. The question as to what E_T value to use for a given background luminance deserves further evaluation. The merits of the BLEU data compared to that of Blackwell, or others, should be assessed.

3. The effects of multiple light sources as visual cues deserves further attention. Allard's Law visibility calculations are presently based on the characteristics of a given target light. In reality, such a light is always part of a more complex pattern, for example, the five lamps on one approach light bar. This leads to questions of summation on the retina, veiling luminance, and other physiological effects.

4. The definitions relating to concepts of slant visibility deserve further attention. The Slant Visual Range (SVR) refering to visibility along the glide path seems inappropriate because the pilot does not look along the glide path for his visual cues. The glide path intersects the runway 1000 ft from

threshold. To see the approach lights, the line of sight has to be below the glide path. The Visual Guidance Segment (VGS) and Approach Light Contact Height (ALCH) definitions are problematic since they do not refer to the true cockpit cutoff angle of the particular aircraft. As such, they could be very misleading. On the other hand, a definition should be universal, and not involve any reference to a particular aircraft geometry.

5. With regard to a future visibility measuring system, the following considerations apply.

At this point more experimental field work is required to verify the ingredients of the analysis. This is particularly true for the atmospheric model considerations, the γ-β question under various atmospheric conditions, and the problem of inhomogeneities. A complete and reliable theory of the signal processing which can account for the variety of atmospheric conditions must be developed, and the background radiance under the most unfavorable conditions should be studied and measured.

Only after these preliminary aspects are completed, can a meaningful systems analysis and optimization be performed and tested. The results of a successful test program then lead to specifications of a working visibility measuring system.

REFERENCES

1. W. E. Knowles Middleton, Vision Through the Atmosphere, U. of Toronto Press 1952.

2. H. C. Van DeHulst, Light Scattering by Small Particles, John Wiley & Sons, Inc., Landon-Sidney 1957.

3. ESSA- Weather Bureau, Air Weather Service and Naval Weather Service, April 1966. Manual of Surface Observations (WBAN) Circular N, Washington, D.C.

4. Federal Aviation Agency, Feb. 24, 1965, Runway Visibility Measurements, Circular AC No. 00-13A., Washington, D.C.

5. Surface Observations, Abridged form, Federal Meteorological Handbook No. 1., FAA, LAWR, SAWR, and A-type stations, U.S. Department of Commerce, Environmental Science Services Administration Weather Bureau, Silver Spring, MD.

6. H. R. Blackwell, Contrast Thresholds of the Human Eye, J. Opt. Soc. Am 36, 1946, 624-642.

7. H. A. Knoll, R. Tousey, E. O. Hurlburt, Visual Thresholds of Steady Point Sources from Dark to Daylight. J. Opt. Soc. Am. 36, 1946, 480-482.

8. An Analysis of Runway Visual Range RD-66-100, December 1966.

9. Assessment of Visual Range on Runways, D. C. Thomas, Journal of Science & Technology, Vol. 37, No. 2, 1970, pg. 65.

10. C. A. Douglas, National Bureau of Standards Report 2715.

11. DOT-FAA Engineering Requirement FAA-ER-450-042a.

12. S. Chandrasekar, Radiative Transfer, Dover Publications, New York 1960.

13. Classical Electricity and Magnetism., W. K. H. Panofsky and M. Phillips. Addison-Wesley Publishing Co., Inc., Cambridge, MA 1955.

14. S. Twomey and H. B. Howell, Applied Optics 4, No. 4, April 1965.

15. J. A. Cucio and G. L. Knestrick, JOSA 48, No. 10, pg. 680, 1958.

16. Backscatter Signature Studies for Horizontal and Slant Range Visibility, R. T. Brown, Final Report RD-67-23 prepared for FAA-SRDS, May 1967.

17. Visibility Measurement for Aircraft Landing Operations, R. T. H. Collis, et al. Final Report AFCRL-70-0598, prepared for the U.S. Air Force and the FAA.

18. Laser Communications System, William K. Pratt, John Wiley & Sons, Inc., New York, 1969.

APPENDIX A

VISUAL FACTORS IN THE DETECTION OF POINT SOURCES FROM AIRCRAFT

This Appendix was written by
R. T. Mitchell
The MITRE Corporation
Bedford, Mass.

under a contract with DOT/TSC.

APPENDIX A

TABLE OF CONTENTS

INTRODUCTION

A aircraft intending to land approach airports under ground control, ground personnel transmit an estimate of visual range to the aircrews. This is an estimate of the range at which a crewman may expect to see a certain landmark or landmarks essential to the landing process. One method of calculating visual range combines a chosen value of the visual threshold with measurement of the atmospheric transmissivity in a relationship known as Allard's Law to predict the range at which an approach or runway light of given intensity will just exceed an observer's threshold. One such estimate, called Runway Visual Range, uses two values of threshold illuminance, 1000-mile candles for daylight and two-mile candles for nighttime. Data collected from aircrew reports[1] and from an experiment using stationary observers on the ground [2] show great variability in the indicated threshold illuminance with the range of values typically in excess of five or six log units for both the day and night conditions. The following is an attempt to describe properties of the human visual system and their interactions with the visual environment which are relevant to both choosing values of the visual threshold to be used in predicting sighting ranges, and evaluating a possible source of the variability.

FACTORS AFFECTING DETECTION OF DISTANT STEADY POINT SOURCES

Illuminance at the Eye and Background Luminance

The principal factors governing the detection of distant steady point sources whose position is known within small angular limits are: the illuminance, E, at the observer's eye and the background luminance, B_0 , of the immediate surround of the source of interest.

E is a function of three factors: the intensity, I, of the source in the direction of the observer; the distance, r, between source and observer; and the transmittance, T, of the atmosphere over the distance, r. For a homogeneous atmosphere, T may be calculated from the transmissivity, t, and the illuminance is given by Allard's Law: $E_r = It^r/r^2$.

B_0 is a function of the directional reflectances of the area of interest and the intensities and positions of the sources which illuminate it. Analytic treatment of B_0 for varying surfaces illuminated by complex natural and/or artificial sources is impossible over the gamut of possible conditions. However, some reasonable bounds can be readily chosen for the case of natural illumination on the basis of existing measurements. It is convenient for discussion to designate three categories of illumination, even though the boundaries between them are necessarily somewhat arbitrary. These are: day, night and the periods of transition between them. The bounds chosen here for day are 10 ft-L and 8,000 ft-L, the former representing a low-to-medium reflectance surface on an overcast day, and the latter fresh snow on a clear day. Night is here taken to span the range from 0.000001 ft-L to 0.01 ft-L, the former representing earth on a moonless night and the latter snow in full moonlight. The range from 0.01 ft-L to 10 ft-L, then, is the transition region.

With these boundaries as guides, one can use existing experimental data to estimate the ranges of threshold illuminance, E_t , for the three categories of illumination. The data of Blackwell[3] are most frequently used for this purpose. His data for a target subtending 0.595 minutes of angle are recomputed to yield the total

E_t (instead of the threshold increment), and a correction factor is applied to compensate for the fact that the reported values are for a 50% probability of detection.

In the present case, however, the estimates will be based on the data of Knoll, Tousey and Hulburt[4]. The latter were chosen because the experimental conditions more closely resemble field conditions: binocular vision, natural pupil, non-constrained fixation and instructions to adjust the stimulus intensity "until it is just visible all the time." Actually, the choice is of little consequence since these data agree very closely with those of Blackwell if the latter are adjusted to take account of the 50% criterion.[1]

The empirical relationship found by Knoll et al is shown in Figure 1. From this one may determine that E_t for the lowest night background is -2.2 log mile candles and for the brightest day background, 3.8 log mile candles; a spread of 6 log units. Not all of this range is applicable to detection of approach or runway lights from an aircraft on final landing approach.

Here we digress to describe briefly the dual nature of the human visual process. It consists of a photopic system and a scotopic system, mediated in part by two functionally different types of receptors in the retina: the cones and rods. The names of these receptors arose from anatomical differences, but should

---

[1] This statement is in disagreement with Middleton[5], pp. 97-98. Middleton recomputed the Blackwell results to total E_t but neglected to do so for the Knoll et al data, which led to his conclusion that they did not agree at higher values of B_0.

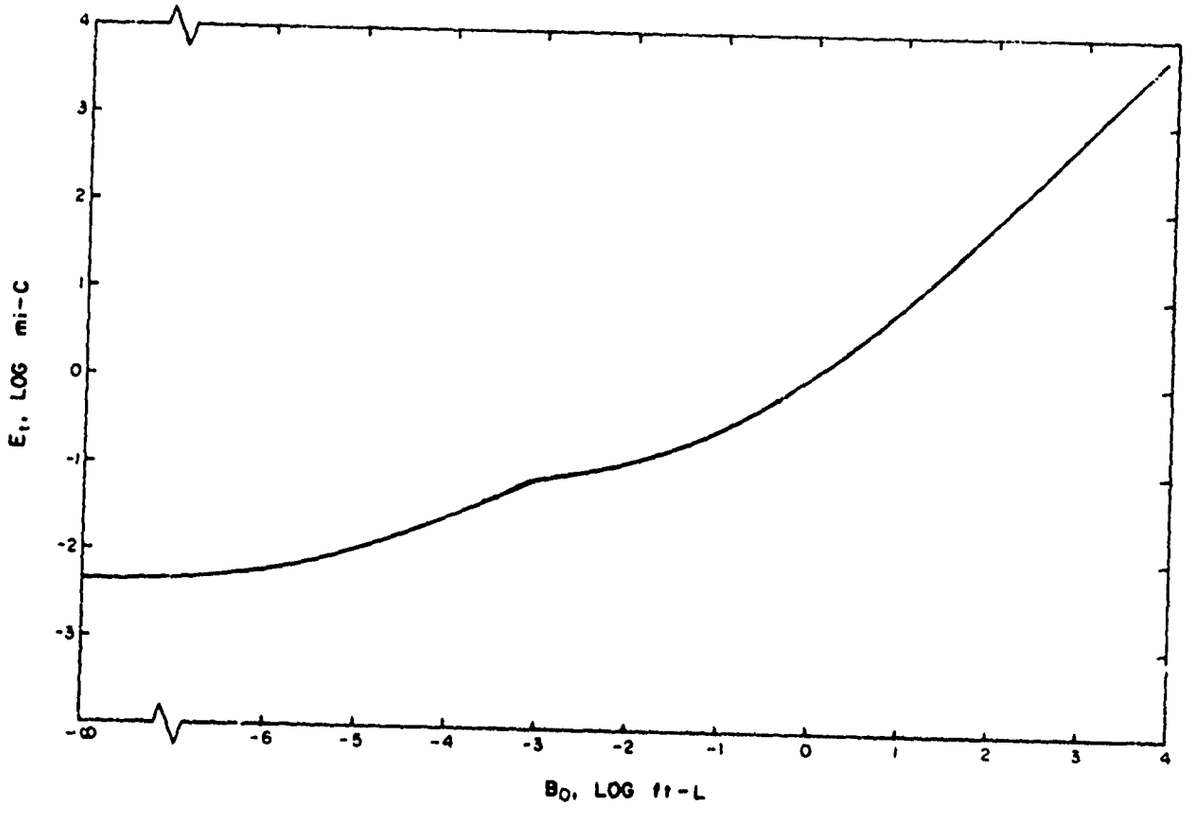

Figure 1 THRESHOLD ILLUMINANCE AS A FUNCTION OF BACKGROUND LUMINANCE (AFTER KNOLL, TOUSEY & HULBURT)

not be taken too literally, since the "cones" which are tightly packed in the region where the visual axis of the eye meets the retina are really more rod-shaped than are the "rods". The photopic system (cones) is dominant at higher levels of luminance, and is associated with the perception of color and with maximum visual acuity. The scotopic system (rods) dominates at light levels below those to which the cones can respond, and is associated with lack of color vision and relatively poor acuity.

The retinal distribution of the two types of receptors differs. The maximum density of cones occurs in a small area -- approximately 1/2° in diameter -- about the visual axis called the fovea, with the density decreasing rapidly out to about 20° off-axis and thereafter remaining stable at a low level. There are few if any rods in the fovea; their density increases rapidly out to about 20°, then declines again toward the periphery of the retina. From 0 to 5° eccentricity visual acuity is proportional to the density of cones. Beyond this region acuity is progressively poorer than would be predicted by cone counts. This suggests that there is a functional area whose cone receptors have a constant ratio (perhaps 1:1) of representation in the data-processing department, and that more peripheral receptors increasingly share "party lines".

The separation of the two systems by light level may be seen in Figure 1 where the limb to the right of the inflection at -3.0 log ft-L represents photopic function, and that to the left, scotopic. This Figure also shows that the 1.0 log unit rise in

threshold illuminance between backgrounds of -6.0 and -3.0 log ft-L is within the scotopic system.[2]

The position taken here is that the detection of the lights of interest is a photopic foveal task.[3] Since the minimum photopic threshold, -1.2 log mi-c, is associated with a B_0 of -3.0 log ft-L, lower values of B_0 will not result in lower values of E_t for the task of interest. This adjustment in the minimum E_t value decreases the total expected range of E_t from 6.0 to 5.0 log units.

Ranges of values of B_0 and their associated E_t values are shown in Table I. The E_t values in Figure 1 and this Table are based upon observations under laboratory conditions by trained subjects; therefore it is of interest to compare them with data gathered under field conditions.

---

[2] Most comparisons of the lower thresholds of the photopic and scotopic systems state that the latter is 2.5 to 3 log units lower, whereas the difference shown in Figure 1 is only 1.0 log unit. The discrepancy arises from the fact that the usual visual threshold test stimulus has considerable angular extent, typically two degrees or more. The magnitude of areal summation in the scotopic system is much greater than in the photopic system. When the stimulus is a point source, areal summation cannot occur (except over the Airy disc) and the threshold difference is smaller.

[3] It may be argued that point sources, such as stars, can be detected at low levels using extra-foveal vision when they cannot be seen with the fovea. However, in the landing-approach situation a particular group of lights must be perceived as a pattern in order to discriminate them from other possible sources in the area. The limited acuity and unstable fixation of dark-adapted extra-foveal vision would make such a discrimination very difficult if not impossible.

TABLE I

Background Luminances and Corresponding Threshold Illuminances for Point Sources Under Three Categories of Illumination

		DAY	TRANSITION	NIGHT
B_0	max.	8,000 (3.9)	10 (1.0)	0.01 (-2.0)
ft-L (log ft-L)	min.	10 (1.0)	0.01 (-2.0)	0.000001 (-6.0)
E_t	max.	6,500 (3.8)	8 (0.9)	0.1 (-1.0)
mi-c (log mi-c)	min.	8 (0.9)	0.1 (-1.0)	0.06 (-1.2)

Lefkowitz and Schlatter[2] report an experiment carried out at the National Aviation Facilities Experimental Center (NAFEC) at Atlantic City. Observers on a platform about eight feet above the center of a runway reported the most distant runway light they could see. Transmissivity measurements and background luminances were recorded at the time of each observation. Threshold illuminance for each observation was calculated by Allard's Law. Observations were carried out over the period from September 1, 1965 to May 15, 1966 and were limited to conditions of t <.80 during the day and t <.50 at night with t measured over a 500 ft. baseline. Thirty observers participated for varying numbers of observations, totaling 990 in daylight and 1511 at night. The demarcation between day and night was chosen to be at B_0 = 2 ft-L.

Data from Figure 20 of Lefkowitz and Schlatter are shown here in Figure 2. The night thresholds range from -2.6 to 4.2 log mi-c with a median of -0.1. Day thresholds range from -0.6 to 4.5

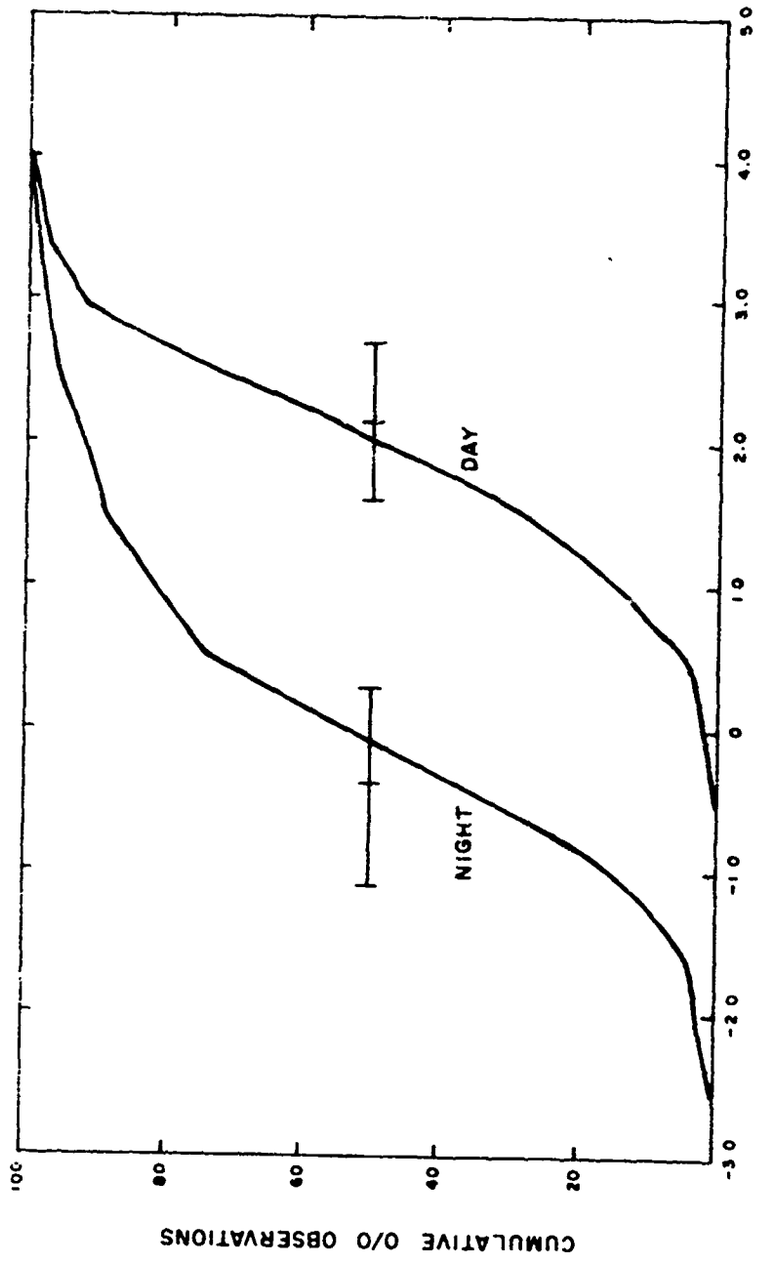

Figure 2 CUMULATIVE SIGHTINGS OF RUNWAY LIGHTS AS A FUNCTION OF ILLUMINANCE AT THE EYE (AFTER LEFKOWITZ AND SCHLATTER)

log mi-c with a median of 2.0. Reported values of B_0 fell between 0.002 and 2.0 ft-L for night observations and between 55 and 910 ft-L for day. From these we may determine the limiting values of E_t predicted by the Knoll et al experiment. These are approximately -1.1 and 0.3 log mi-c for night and 1.6 and 2.7 for day, and are shown in Figure 2 as the end points of the horizontal bars. As may be seen, the midpoints of these ranges agree quite well with the medians of the NAFEC observations and the ends enclose 56 and 48 percent of the night and day data respectively.

The aspect of the field data which corresponds poorly with the laboratory results is that of the ranges: 6.6 versus 1.4 log units for night and 5.1 versus 1.1 log units for day. It can be argued that E_t values measured in the field which exceeded the upper limit of the laboratory values arose from the numerous factors which might have been present to degrade performance from optimum. However, this argument cannot cope with the 32% of the day cases in which the reported E_t was less than laboratory threshold for the lowest B_0, 55 ft-L. The lowest day E_t value is 2.0 log units below the laboratory value corresponding to B_0 = 55 ft-L. No known properties of the visual system could account for this result. Because of the correspondence of midpoints, it is tempting to speculate that the distributions of the field data arose from a combination of the threshold characteristics of the visual system and some source of random variation which is normally distributed with a mean equal to zero. At any rate, one must conclude that the known variation of E_t as a function of B_0 does not account for the variance of the distribution of calculated E_t based upon the observations collected by Lefkowitz and Schlaer.

The entries in Table I are based on measurements of the range of B_0 due to natural illumination. Artificial sources at or near an airport would have little effect in daytime but could significantly raise B_0 at night. The range of total illuminance at night at large civil airports was found by Rose[6] to be from 0.002 to 0.05 ft-c. Assuming a reflectance of 0.5, B_0 would range from 0.001 to 0.025 ft-L and E_t from 0.06 to 0.16 mi-c. These data strongly reinforce the position taken earlier that the task of interest is strictly limited to the photopic visual system. The observer's aircraft may also contribute to B_0. Examples are specular reflection of the cockpit luminance from the windshield, and backscatter if landing lights are used during fog or precipitation.

Other Factors

In addition to the factors of illuminance at the eye and background luminance discussed above, there are other aspects of the stimulus situation which have potential for affecting detection thresholds. These may, for convenience, be divided into spatial effects and temporal effects, though any given situation may partake of both classes. In the previous discussion it has been tacitly assumed that the target of interest appeared on backgrounds which were of considerable angular extent and were relatively stable over time. We will now examine some tuations in which these conditions do not hold.

Spatial Effects

Spatial effects may be characterized as interactions occurring when there are spatial inhomogeneities in the distribution of

luminances in the visual field. These effects arise from differences between the distributions of luminance in the visual field and of illuminances on the retina as a result of scattering in the ocular media, and from interactions which take place in the visual system after energy is absorbed. The former condition will be discussed later along with other aspects of "glare".

Spatial interaction of the second type in the visual field is a very complex topic and, because of the multitude of stimulus patterns which can exist, is still incompletely described despite the existence of much experimental data. No practical strategy for selecting E_t values and predicting sighting ranges at airports could hope to cope with the possible variations arising from local terrain, ground cover, sun angle, time of year, etc. Fortunately, these interactions are less marked, and span less angular separation, for foveal than for extra-foveal stimuli.

A straightforward question can be asked concerning the effect of an adjacent boundary upon the threshold of a foveal stimulus. While Knoll et al collected their principal data with the test stimulus centered on a circular background subtending 12°, they also investigated the effect of decreasing the background to 0.8° (leaving the rest of the field dark), and of moving the test point about on a large background to within 0.4° of the boundary. No differences in the E_t , B_0 relationship were found from the case of the large, centered surround, indicating that any boundary effect in the fovea does not spread far. However, these data are limited to the condition where the threshold stimulus occurs in the lighter portion of the field.

An experiment by Fiorentini and di Francia, reported by Brown and Mueller[7], sheds further light on the question. These experimenters employed adjacent light and dark fields having a luminance ratio of 80:1 with a narrow, 0.067° gradient between. Threshold for a small test patch was measured as it was translated across the boundary. The threshold was highest where the gradient met the lighter field -- approximately twice as large as when the background was the lighter field. Of particular importance was their finding that the boundary effect was sharply peaked, with the threshold dropping to baseline level within 0.08° to either side of the point of maximum effect. In summary, we can say that the presence of boundaries in the vicinity of a target of interest should not present a problem in predicting sighting range; an "edge" effect occurs only if the target is almost precisely at the boundary, and then the effect is small compared to other sources of variance present in a field situation.

The other class of spatial effects consists principally of conditions in which there are one or more sources in the visual field whose luminance is greater than the background against which the target of interest must be discriminated. Such conditions are usually discussed in connection with glare, but it should be recognized that elevation of the threshold for a weak target is not limited to cases where there are concentrated sources of high intensity. Any source which has higher luminance than the immediate surround of the target may produce an effective increase in the luminance of the background and hence in the target threshold. Part of this increase in B_0 has been shown to be due to scattering by the cornea and other ocular media, but there appears to be an additional inhibitory effect whose origin is speculative. At any

rate, the effective background luminance B_0' for which an appropriate E_t must be selected is equal to $B_0 + \beta$. β is a function of θ, the angular separation of the source from the target, and E, the illuminance it produces at the observer's eye. LeGrand[8] gives an empirically determined relationship:

$$\beta = 10E\theta^{-2}$$

where E is in lumens per unit area, β is in candelas per unit area and θ is in degrees. Effects due to multiple sources can be summed to give the total B_0'.

Using this relationship, one can approach the question of the effect of the luminance of cockpit instruments on the detection of external point sources. In Figure 3 the four quadrilaterals with heavy outlines represent the angular extents and positions of the windshields of a DC-9 aircraft as seen from the captain's seat, as given by reference (9). The + symbol on the captain's front windshield indicates his line of view parallel to the axis of the aircraft. The concentric circles about the + indicate 20° angular increments in the visual field. The shaded areas above and below the three rightmost windshields represent estimates of the visual areas containing instruments. For purposes of analysis these instrument areas have been divided, as indicated, into 20 sub-areas and the visual effect of each sub-area assigned to the angular position of the center of that sub-area. If the effective luminances, B_s, of the sub-areas are assumed to be equal, β at the line of view may be calculated by:

$$\beta = B_s \, 10 \sum_{i=1}^{n} \omega_i \, \theta_i^{-2}$$

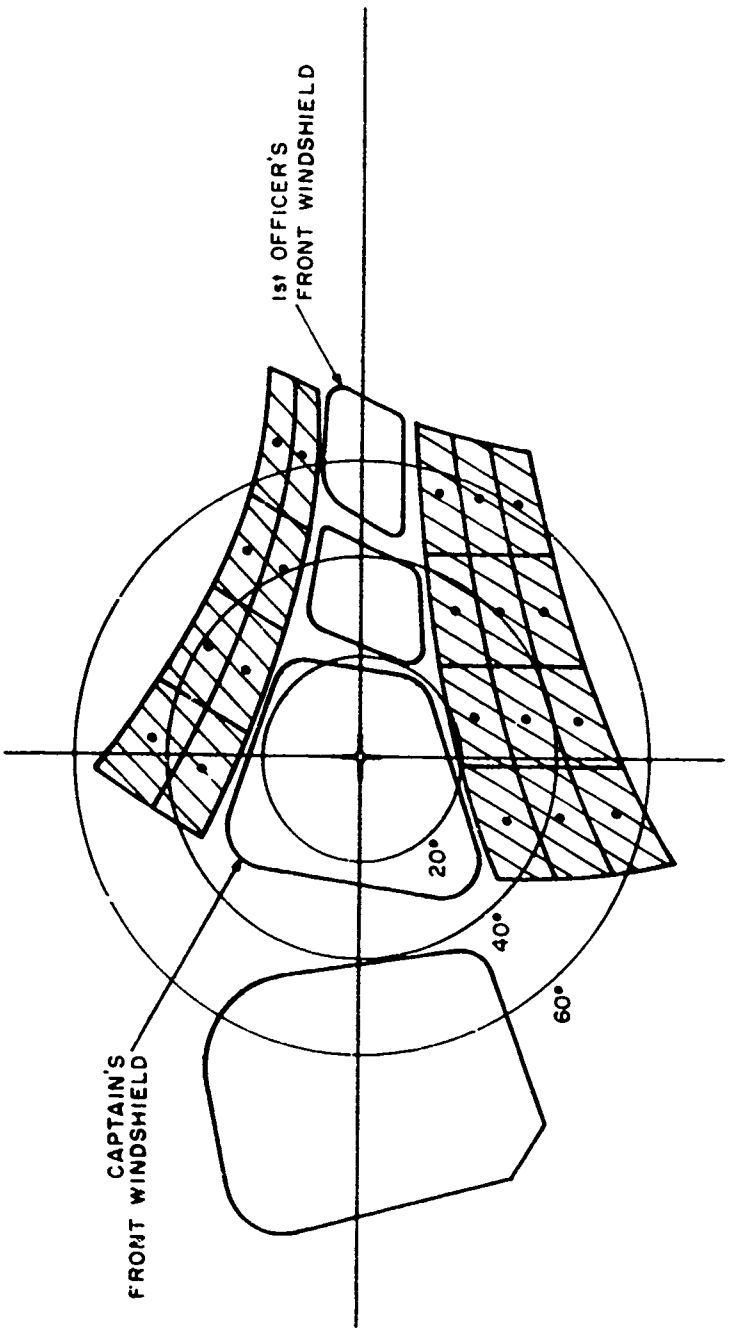

Figure 3 VISUAL FIELD FROM LEFT-HAND SEAT IN DC-9 COCKPIT

where ω is the subtense of sub-areas in steradians, θ the angular separation of their centers from the line of view, and β and B_s can be any convenient units of luminance so long as they are the same. Carrying out the summation and multiplying by 10 gives the weighting factor 0.0079 for the example depicted in Figure 3.

Data from Dohrn[10] provide a basis for estimating B_s. Dohrn measured the luminances of pointers and numerals of instruments at night in seven types of military aircraft. Highest luminances were found in a C-124, the type among those measured most likely to resemble multi-engined commercial aircraft. The brightest portion of the brightest instrument averaged over several measurements was found to be 0.37 ft-L at normal intensity setting for night flying in the C-124. Bearing in mind that this was the highest luminance measured and that the light area of most instruments represents only a relatively small proportion of their total area, 0.37 ft-L may be used in conjunction with the weighting factor obtained to provide a very-worst-case estimate of $\beta = 0.0030$ ft-L.

Taking B_0 equal to 0.001 ft-L, the lowest level which affects the foveal E_t and for which $E_t = 0.06$ mi-c, $B_0' = B_0 + \beta = 0.004$ ft-L and E_t increases to 0.08 mi-c. This would result in a decrease of 18% in the sighting range considering only the inverse-square component of Allard's Law. Whether a decrease of this magnitude is significant, in view of the large variance found in reported sightings, is problematical. As B_0 increases, the effect of a β of 0.0030 is quickly nullified. A more realistic estimate of the effect of instrument lighting may be made by considering the fact that most instruments have small lighted areas on large dark

grounds. If we estimate conservatively that the lighted portion is 10% of the total, the average luminance of the areas in question becomes 0.037 ft-L, β is 0.0003 ft-L, and the effect on B_0' and E_t is negligible.

It should be borne in mind that the above conclusions regarding the effect of instrument lights are limited to foveal targets. For the task of detecting a relatively large target against a very dark background using extra-foveal vision the effect of a β of 0.003 or even 0.0003 ft-L could be substantial.

There may also be other sources in the environment more commonly thought of as glaring. Examples are the sun and moon at low zenith angles, and the sun reflected from standing water or from the windshield. The appropriate β can be computed for any specified set of conditions. For instance, on a very clear day the sun at a 70° zenith angle produces 8,500 ft-c on a surface normal to the direction of the sun. The resulting β for a target of interest at an angle of 25° from the sun is about 400 ft-L. However, it is not readily apparent how provision for such conditions can be included in a procedure for estimating sighting range without producing intolerable complication.

Temporal Effects

The relationship of temporal visual effects to the design and control of cockpit lighting has long been the subject of intense interest. Most effort has been concentrated on preserving maximum dark-adaptation at night, usually by controlling the intensity and spectral power distribution of the cockpit illuminant.

The relationship describing the change in sensitivity of the visual system as a function of time in the dark is usually presented as shown by the solid curve in Figure 4. The initial recovery is rapid, becoming progressively slower, followed by a rather abrupt transition to more rapid recovery which again becomes progressively slower. The early limb of the curve is associated with the photopic system and the second limb with the scotopic system. If the pre-adapting luminance is reduced, the recovery is as shown by the dashed curve in Figure 4. Here the photopic segment is not apparent and scotopic recovery starts earlier, but slows, eventually becoming indistinguishable from recovery after exposure to the higher luminance. If the test stimulus is confined to a rod-free area of the fovea, only the photopic recovery is measured, and the threshold would remain at about three log units in the examples shown.

In the aircraft situation being considered, recovery from adaptation to high luminances normally presents no problem, since the natural transition from daylight to night is very much slower than the photopic changes of sensitivity. The condition of chief concern is therefore the transition from viewing the illuminated cockpit to attempting to detect dim external lights. As stated earlier, there has been considerable applied research concerned with cockpit lighting and dark-adaptation, but attention has been almost entirely confined to the scotopic system. Further, there is a dearth of more general laboratory studies on photopic thresholds following exposure to low- and medium-level luminances. The effects are too small to have excited much interest, and so brief as to be difficult to measure. However, there are data which appear to provide satisfactory answers.

Baker, Debons and Morris[11] have shown that if an observer scans an adapting field composed of a large number of small light

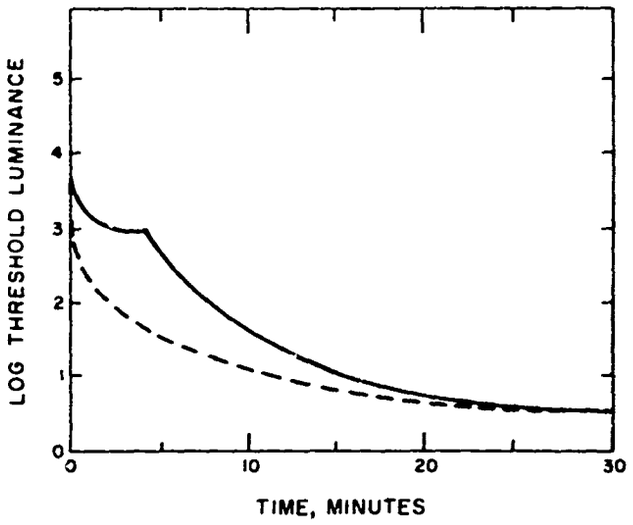

Figure 4 TYPICAL DARK ADAPTATION CURVES

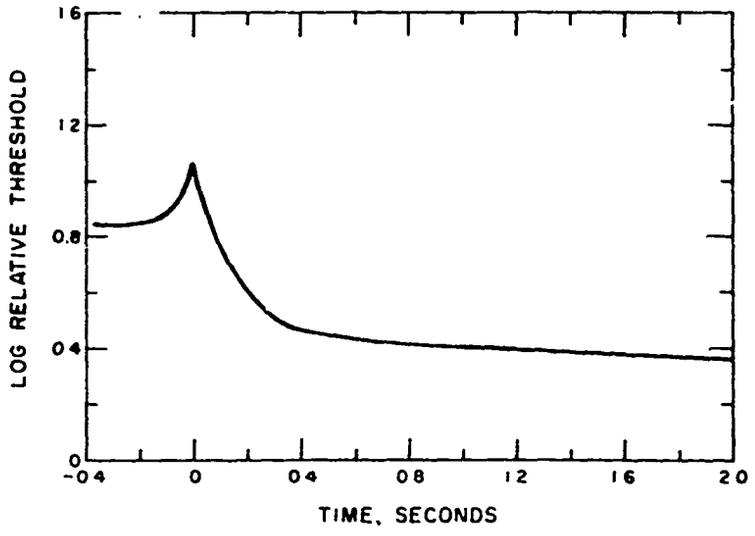

Figure 5 EARLY COURSE OF FOVEAL THRESHOLD (AFTER BAKER)

areas in an otherwise dark field, the adapting effect is given by the product of the luminance of the light areas and the proportion of the area of view they occupy. This finding, together with Dohrn's measurements, provide estimates of the adapting effect of an aircraft instrument panel. As before, if one assumes the entire instrument panel to be illuminated to the highest level found by Dohrn for the brightest part of the brightest instrument, one gets 0.37 ft-L as a very worst case and 0.037 ft-L as a more probable figure, based on the estimate that 10% or less of the panel is actually illuminated.

Johannsen, McBride and Wulfeck[12] measured the time course of the foveal threshold following ten minutes exposure to a 1.0 ft-L field and found no measurable elevation as compared to the fully dark-adapted threshold. These data are somewhat limited, since the experimental method precluded measurements sooner than about four seconds after the adapting field was removed. Baker[13] provides data on the behavior of the foveal threshold during and immediately following the cessation of an adapting field. Baker's lowest adapting field was reported to give a retinal illuminance of 57 trolands. From the data of Reeves[14], relating pupil size to luminance, the corresponding luminance with a natural pupil can be computed as approximately 0.9 ft-L. The threshold data for this luminance are shown in Figure 5, which shows that about 6 db of sensitivity is recovered in the first 0.4 seconds after cessation of the adapting light and a further 1 db during the next 1.6 seconds. Noting that there is about a 2.5 db decrease in sensitivity at the instant the adapting field is turned off, one may speculate that the rapid recovery in the first 0.4 seconds results from a combination of the dying away of the burst of neural "off-pulses" with the 3.5 db increase in retinal illumination resulting from pupil dilation.

It is unfortunate that the measurements did not extend a few seconds beyond 2.0 seconds, but the Johannsen et al result cited above, combined with these data, indicate that any effect of an adapting field of 1.0 ft-L effective luminance, or less, after the first half second of removal is small. Nor is the brief initial effect of concern, because an aircrewman shifting attention from cockpit to outside would have to make a visual accommodation change of about two diopters to bring a point source into focus -- a process which itself requires more than one-half second[15]. Therefore it is concluded that the light-adaptation induced by normal cockpit lighting will not adversely affect the threshold illuminances for point sources viewed foveally.

There may be sources of light-adaptation in the cockpit other than instruments. One that comes readily to mind is a light-colored checklist read under a small spotlight. Depending on the luminance level, this could adversely affect detection performance for up to two minutes afterward. Another experiment by Johannsen, McBride and Wulfeck[16] indicates that if the adapting luminance in ft-L does not exceed 1.0 or if the product of luminance and duration in seconds does not exceed 100, the effect on the foveal threshold will be negligible. At any rate, it is clear that the management of this and other such bright objects should be a matter of cockpit discipline and not a basis for altering sighting range predictions made from the ground. Lightning flashes are another occasional source of transient light adaptation not readily amenable to prediction.

The use of red illuminants in cockpits has long been popular and is still the subject of much discussion[17]. Any benefit in preserving or facilitating dark-adaptation by restricting illuminants

to longer wavelengths arises solely from the relatively lower sensitivity of the scotopic system to long-wavelength energy as compared to the photopic system. To the extent that the C.I.E. luminosity function and the assumptions underlying the photometric system based upon it are valid, any and all spectral power distributions of equal luminance will have equal effect on the state of adaptation of the photopic system. Therefore discussion of the merits and demerits of red lighting is not germane here.

Temporal effects also occur when an observer who is adapted to a low level of luminance is abruptly shifted to a higher level as might occur when an aircrew member who has been working "inside the cockpit" begins to search for a light source against a brightly sunlit background. Baker[18] investigated the case of observers first adapted to full darkness and then required to detect a threshold target against a luminous field. A substantial sensitivity decrement was found immediately following the introduction of the test condition. He was unable to obtain stable data during the first few seconds, so the magnitude of the decrease is uncertain; but it is clear that the loss increased as the luminance of the conditioning field increased. Initial recovery was rapid but became slower, and from one to two minutes delay, depending on the luminance of the field, occurred before maximum sensitivity was achieved. Unlike Baker's subjects, of course, an aircrewman would not be adapted to full darkness and the effect would be less severe. But the exact amount of loss is uncertain, since no data were found on the effect of shifting from an intermediate to a higher level. Some shaky extrapolation from the Baker results leads to the estimate that the decrease in sensitivity from the eventual steady-state level should not exceed 2 db ten seconds after shifting to the brighter background.

SUMMARY

The properties of the human visual system have been examined with respect to the prediction of sighting ranges from aircraft to point sources of illumination whose direction is known. It was concluded that the task of interest is limited to the foveal photopic visual system. Available data indicate that the threshold illuminance at the eye can vary over a five log unit range (0.06 to 6,500 mi-c) as a function of the background luminance produced by natural illumination. The sources of artificial illumination typically associated with airports raise the background luminance at night and an increase in the minimum threshold to as high as 0.16 m -c may result. Data gathered in a field study at NAFEC using stationary observers on the ground show a far greater variability in the computed threshold than can be accounted for by the range of background luminances which were measured. The source of this variability was not identified.

Spatial effects within the visual field such as contours, or the veiling luminance produced by cockpit instruments, were shown to be of little or no consequence. Strong glare sources, such as the sun's disc or its reflection from windshield or standing water, are probably too unpredictable in time and space for practical inclusion of their effects in a prediction algorithm.

Temporal effects can occur during shift from a darker to a lighter field or vice versa. Scanning instrument panels should not adversely affect the detection of external point-source targets of interest at night. Viewing brightly lit objects of high reflectance in the cockpit, on the other hand, could do so, and such objects should be eliminated by equipment design and operational rules.

Shifting gaze from the darker cockpit to a brightly daylit exterior will cause some loss of sensitivity. The magnitude of loss is uncertain because of lack of experimental data, but recovery should be virtually complete after a few seconds.

APPENDIX A

REFERENCES

1. W. E. Eggert, Approach Visibility Studies at Newark, Federal Aviation Agency, AMB Project D-1-902 Final Report, September, 1960.
2. M. Lefkowitz and E. E. Schlatter, An Analysis of Runway Visual Range, Federal Aviation Agency, Report No. RD-66-100. December, 1966.
3. H. R. Blackwell, Contrast Thresholds of the Human Eye, J. Opt. Soc. Am., 36, 1946, 624-643.
4. H. A. Knoll, R. [illegible]ey and E. O. Hulburt, Visual Thresholds of Steady Point Sources from Dark to Daylight, J. Opt. Soc. Am., 36, 1946, 480-482.
5. W.E.K. Middleton, Vision Through the Atmosphere, Univ. Toronto Press, Toronto, rev. ed., 1958.
6. H. W. Rose, Luminance of the Horizon and Dark Adaptation during Meteorological Observations, USAF School of Aviation Medicine, Project 21-02-144, Report No. 1, 1950.
7. J. L. Brown and C. G. Mueller, Ch. 9 "Brightness Discrimination and Brightness Contrast" in Vision and Visual Perception, C. H. Graham ed., John Wiley & Sons, New York, 1965.
8. Y. LeGrand, Light, Colour and Vision, John Wiley & Sons, New York, 1957.
9. National Transportation Safety Board Aircraft Accident Report, SA-396, June 19, 1968.
10. R. H. Dohrn, Luminance Measurements of Red and White-Lighted Aircraft Instruments, AGARD Conference Proceedings, No. 26, October, 1967.
11. C. A. Baker, A. Debons, and D. F. Morris, Dark Adaptation as a Function of the Intensity and Distribution of Light Across the Preadaptation Field, J. Opt. Soc. Am., 46, June, 1956, 401-404.

12. D. E. Johannsen, P. I. McBride and J. W. Wulfeck, Studies on Dark Adaptation II, The Pre-exposure Tolerance of the Human Fovea Adapted to Different Brightness Levels, J. Opt. Soc. Am., 46, 1956, 266-269.

13. H. D. Baker, The Instantaneous Threshold and Early Dark Adaptation, J. Opt. Soc. Am., 43, 1953, 798-803.

14. P. Reeves, The Response of the Average Pupil to Various Intensities of Light, J. Opt. Soc. Am., 4, 1920, 35-43.

15. W. D. Zoethout, Physiological Optics, The Professional Press. Inc., Chicago, 1947.

16. D. E. Johannsen, P. I. McBride and J. W. Wulfeck, Studies on Dark Adaptation I, The Pre-Exposure Tolerance of the Dark-Adapted Fovea, J. Opt. Soc. Am., 46, 1956, 67-71.

17. Aircraft Instrument and Cockpit Lighting by Red or White Light, Advisory Group for Aerospace Research and Development - NATO, AGARD Conference Proceedings No. 26, October, 1967.

18. H. D. Baker, The Course of Foveal Light Adaptation Measured by the Threshold Intensity Increment, J. Opt. Soc. Am., 39, 1949, 172-179.

APPENDIX B

EYE SAFETY REQUIREMENTS

EYE SAFETY REQUIREMENTS

It is clear that any system involving optical lasers which is operated in open installations can be a severe eye hazard. This fact must be taken into consideration when laser systems are proposed for visibility measurements, or other purposes, at airports. Fortunately, the intensities required for our purposes are not crucial, and one can always reduce the intensity by increasing the cross section of the outgoing beam while keeping the total power or energy constant.

An excellent review, Ocular Hazards from Lasers and Other Optical Sources by A. M. Clarke* appeared recently. This paper pointed out that there is no particular consensus as to what the permissable exposure values are. The Table on the following page summarizes the results of three different guidelines discussed by Clarke. We apply the guidelines set by the U.S. Surgeon General's Report.**

---

*A. M. Clarke, CRC Critical Reviews in Environmental Control, Nov. 1970, pg. 306.

**Department of the Army and Department of the Navy, TB-MED 279/NAVMED P-5052-35 Control of Hazards to Health from Laser Radiation, Washington, D.C. Feb. 1969.

TABLE 1. EYE SAFETY - MAXIMUM EXPOSURE LEVELS. (ACGIH = AMERICAN CONFERENCE OF GOVERNMENT INDUSTRIAL HYGIENISTS)

	U. S. SURGEON GENERAL REPORT	AIR FORCE	ACGIH
Q - Switched laser T < 1 msec	1×10^{-7} J/cm^2	15×10^{-6} J/cm^2 Ruby 90×10^{-6} " Nd	1×10^{-8} J/cm^2
Non Q - Switched laser	1×10^{-6} J/cm^2	2×10^{-4} " Ruby 10×10^{-4} " Nd	1×10^{-7} J/cm^2
He - Ne CW	1×10^{-6} W/cm^2	10 mW/cm^2	1×10^{-5} W/cm^2

APPENDIX C

Literature Search on "Night Vision, Dark Adaption, and Low Visibility Perception".

covering 1962 to September 23, 1970

NASA Scientific and Technical Information Facility

Chevaleraud, J.; Mercier, A.; Perdriel, G., "Examination of the central visual function among flying personnel over fifty years old", In Revue Des Corps De Sante Des Armees Terre Mer Air, Col. 9, Oct. 1968.

Mercier, A.; Whiteside, T. . D., "Effect of white or red light illumination of the instrument panel on the dark adaptation index", In Revue De Medecine Aeronautique Et Spatiale, Vol. 7, No. 27, 1968 P. 173-175.

Chevaleraud, J.; Mercier, A.; Perdriel, G., "Efficiency of visual functions in relation to the color of light illuminating the instrument panel', In Revue de Medecine Aeronautique et Spatiale, Vol. 7, No. 27, 1968, P. 152-153.

Beck, R. H., "A pilot looks at visibility", In Air Line Pilot, Vol. 37, Oct. 1968, P. 12-16.

Belleoud; Boyer, Y.; Leluan, D., "Study of the effects of anthocyanin glucosides on the night vision of flying personnel etude des effets des glucosides d'anthocyane sur la vision nocturne due personnel navigant", Repr. from Revue De Medecine Aeronautique Et Spatiale, Vol. 6, No. 23, 1967, P. 5-10, 9 Refs.

Memma, N., "Visual aids in airports from the first night flights to the most recent orientation devices for flights under conditions of low visibility", Revista Aeronautica, Vol. 42, Feb. 1966, P. 179-213.

Kim, D. S.; Kim, Y. S.; Rhee, K. U., "The effects of smoking on night vision", Fourteenth PACAF Medical Conference - Professional Papers, Tokyo, Japan, Nov. 30 - Dec. 2, 1964.

Chisum, G. T., Hill, J. H., "Flash blindness - a problem of adaptation", Aerospace Medicine, Vol. 35, Sept. 1964, P. 877-879.

Giu, D. X., "Night vision requirements for combat pilots in South Vietnam" Oslo, Universitetsforlaget, In-Aviation and Space Medicine, Proceedings of the Seventeenth International Congress, Oslo, Norway, Aug. 5-8, 1968, P. 219-222.

Briggs, J., "Visibility variations at London/Heathrow Airport", Meteorological Magazine, Vol. 98, P. 135-138.

Litchford, G. B., "Low-visibility landing. II.", Astronautics and Aeronautics and Aeronautics, Vol. 6, P. 44-56.

Litchford, G. B., "Low-visibility landing. I." Astronautics and Aeronautics, Vol. 6, P. 26-38.

Fehrentz, G., "New Category II approach lighting for Nuremberg Airport", Siemens Review, Vol. 35, P. 373-375.

Beck, R. H., "The hostile environment of low visibility", Air Line Pilots Assn., Air Safety Forum, 15th, Seattle, Wash., Oct. 9-11, 1968.

Marshall D., "Low visibility operation for the SST Concorde using duplicate monitored systems to achieve automatic failure survival", Association Francaise Des Ingenieurs et Techniciens De L'Aeronautique et De L'Espace, Congres International Aeronautique, 8th, Paris, France, May 29-31, 1967.

Noxon, P. A., "Microvision System 1967", Association Francaise des Ingenieurs et Techniciens de L'Aeronautique et de L'Espace, Congres International Aeronautique, 8th, Paris, France, May 29-31, 1967.

Scano, A.; Terrana, C.; "Red light for cockpit lighting - results of a survey and some experiments", Rivista de Medicina Aeronautica E Spaziale, Vol. 31, P. 34-47.AGARD, Simposio Sull' Illuminazione Rosso-Bianca Della Cabina De Pilotaggio, Brussels, Belgium, Oct. 30, 31, 1967.

Finch, D. M.; Horonjeff, R., "Ground guidance and control in poor visibility", Montreal, International Air Transport Assn., Technical Conference, 17th, Lucerne, Switzerland, Oct. 9-14, 1967. Vol. 2

Smith, D. P., "Runway Visual range at United Kingdom airports", Meteorological Magazine, Vol. 97, P. 51-55.

Brictson, C. A., "Analysis of F4 aircraft day and night carrier approaches", Aerospace Medicine, Vol. 38, P. 1219-1224. Aerospace Medical Assn., 1967. Annual Scientific Meeting, Washington, D. C., Apr. 10-13, 1967.

Schweighofer, H. M., "Instruments for category II approach and transition", Symposium of All Weather Operations, Head Up Displays, Long Range Navigational Aids, Rotterdam, Netherlands, Oct. 13-16, 1965.

Walker, J., "Vehicle movement in bad visibility", International Federation of Air Line Pilots' Associations, Symposium on All Weather Operations, Head Up Displays, Long Range Navigational Aids", Rotterdam, Netherlands, Oct. 13-16, 1965. Volume I.

Coldwell, T., "Initial work on the problem of roll-out and taxying of aircraft in very low visibilities", International Federation of Air Line Pilots, Associations, Symposium on All Weather Operations, Head Up Displays, Long Range Navigational Aids, Rotterdam, Netherlands, Oct. 13-16, 1965, Report Volume 1.

Bressey, P. E., "The pilots' viewpoint on all weather operations", International Federation of Air Line Pilots' Associations, Symposium on All Weather Operations, Head Up Displays, Long Range Navigational Aids, Rotterdam, Netherlands, Oct. 13-16, 1965. Volume 1.

Whiteside, T. C. D., "Visual mechanisms of special importance in aviation", A Textbook of Aviation Physiology. Edited by J. A. Gillies. Oxford, Peramon Press, Ltd., 1965, P. 1004-1013. 7 Refs.

Doxtader, D.; Keston, R.; Massa, R. J., "Visual experiments related to night carrier landing", AC/Lab. for Electronics, Inc., Boston, Mass., Human Factors, Vol. 6, Oct. 1964, P. 465-473, 12 Refs.

Calvert, E. S., "Visual aids in low visibilities", Ministry of Aviation, Royal Aircraft Establishment, Mechanical Engineering Dept., Farnborough, Hants., England. Shell Aviation News, No. 304, 1963, P. 16-19.

Krumeich, K., "The problem of vision during bad weather landing in civil aviation", Arbeits und Forschungsgemeinschaft Graf Zeppelin, Stuttgart, 13 May 1969.

Elworth, C. L.; Kraft, C. L., "Flight deck work load and night visual approach performance", Agard Meas. of Aircrew Performance, Dec. 1969, See N70-19779 08-04.

Brictson, C. A., "Operational measures of pilot performance during final approach to carrier landing", In Agard Meas. of Aircrew Performance, Dec. 1969. See N70-19779 08-04/ Submitted for Publication.

Measurement of aircrew performance - The flight deck workload and its relation to pilot performance. Presented at Symp. held by Aerospace Med. Panel of AGARD at Brooks AFB, Tex., 14-15 May 1969.

Gold, T.; Hyman, A.; "Research in visual perception for carrier landing Technical report, 1964-1968", Sperry Gyroscope Co., Great Neck, NY Avail. CFSTI.

Chaloner, A. B., "Legibility of red and white test objectives and white light", Flying Personnel Research Committee, London, England.

Nurdygin, P. YA., "Methods and some results of experiments on the level of the critical frequency of flashes", Joint Publications Research Service, Washington, D.C.

Donohue, V. R.; Ereneta, W. J.; Gartner, W. B.; Shoemaker, R. E., "Study of flight management requirements during SST low visibility approach and landing operations - volume 1 - Definition of baseline SST landing system", Serendipity Associates, Los Angeles, California.

Scano, A.; Terrana, C., "Red light for cockpit lighting. Results of an inquiry and of some investigations", Agard Aircraft Instr. and Cockpit Lighting by Red or White Light, Oct. 1967.

Lazo, J., "Human factor aspects in aircraft interior lighting", Naval Air Development Center, Johnsville, PA. (Life Sciences Research Group), AGARD Aircraft Instr. and Cockpit Lighting by Red or White Light, Oct. 1967.

Grether, W. F.; Reynolds, H. N., "The effect of red versus white lighting on dark adaptation using a simulated instrument panel for preadaptation", AGARD aircraft Instr. and Cockpit Lighting by Red or White Lihgt, Oct. 1967.

Dohrn, R. H., "Luminance measurements for red and white lighted aircraft instruments", AGARD Aircraft Instr. and Cockpit Lighting by Red or White Light, Oct. 1967.

Dohrn, R. H., "Luminance measurements for red and white lighted aircraft instruments", AGARD Aircraft Instr. and Cockpit Lighting by Red or White Light, Oct. 1967.

Dohrn, R. H.; Kislin, B., "The effect of night cockpit luminance, red and white, on central and peripheral visual performance", AGARD Aircraft Instr. and Cockpit Lighting by Red and White Light, Oct. 1967.

Mercier, A.; Whiteside, . D. C., "The effect of red and of white instrument lighting on the dark adaptation index", AGARD Aircraft Instr. and Cockpit Lighting by Red or White Light, Oct. 1967.

Chaloner, A. B., "Assessment of red and white illumination for equal legibility", AGARD Aircraft Instr. and Cockpit Lighting by Red or White Light, Oct. 1967.

Kinney, J. A. S.; Luria, S. M., "Merits of red or white lighting for naval use", AGARD Aircraft Instr. and Cockpit Lighting by Red or White Light, Oct. 1967.

Mercier, A.; Perdriel, G., "Effect on vision of different modes of instrument panel lighting", AGARD Aircraft Instr. and Cockpit Lighting by Red or White Light, Oct. 1967.

Chisum, G. T., "Color discrimination and chart reading under red and low intensity white light", AGARD Aircraft Instr. and Cockpit Lighting by Red or White Light, Oct. 1967.

Intano, G. P., "Legibility of various sized letters under aviation red "lunar" white, and neutrally-filtered incandescent white lighting systems", AGARD Aircraft Instr. and Cockpit Lighting by Red or White Light, Oct. 1967.

Kurschner, D. "Visual functions as determining factor for quality and amount of effective panel and cockpit lighting", AGARD Aircraft Instr. and Cockpit Lighting by Red or White Light, Oct. 1967.

McVitie, A. M., "Cockpit lighting requirements in the RAF", AGARD Aircraft Instr. and Cockpit Lighting by Red or White Light, Oct. 1967.

"Aircraft instrument and cockpit illumination by red or white light for optimum utilization of pilot visual capabilities". Presented at the Aerospace Med. Panel of AGARD-NATO, Rhode-Saint-Genese, Belgium, 30-31, Oct. 1968.

Betts, L.; Brown, A. D.; Jeffs, N. J., "A Simulator investigation of the problems of visual taxi guidance in low visibilities", Royal Aircraft Establishment, Farnborough, England.

Goddard, C.; Smith, H. A., "Effects of cockpit lighting color on dark adaptation Final report, Apr. 1966 - Jan 1967", Wright-Patterson AFB, Ohio, AF Flight Dyn. Lab., May 1967 83 P.

Biberman, L. M., "Problems in near real time reconnaissance", Institute for Defense Analyses, Arlington, VA. In Mich. Univ. Proc. of the 4th Symp. on Remote Sensing of Environment, Jun. 1966 P. 101-110 Refs.

Gremillet, M. J., "Problems of approach during poor visibility", Feb. 1963, 9 P Transl. Into English of a French Paper Presented at the AGARD Avionics Panel Meeting, Instanbul, 3-8 Oct. 1960.

Rutherford, L. G., "Evaluation of ICAO recommended category II Approach light systems for high performance aircraft Final report", Federal Aviation Agency, Atlantic City, N. J. Mar. 1966 58 P.

Berghage, T. E., Kennedy, R. S., "Pilot attitdues on dark adaptation and related subjects", Naval School of Aviation Medicine, Pensacola, Fla. Jun. 1965.

Levedahl, B. H.; Uyeda, L. R., "Effects of pulsed lighting upon aircraft displays relative to preservation of dark adaptation for night flying" Douglas Aircraft Co., Inc., El Segundo, Calif., Jul. 18, 1962.

Mercier A.; Perdriel, G., "Night vision simulator for pilot training", Advisory group for Aeronautical Research and Development, Paris, France.